ROLE OF WNT SIGNALING

IN ASYMMETRICAL NEURITE PRUNING

IN *CAENORHABDITIS ELEGANS*

by

Menghao Lu

B. Sc., University of Manitoba, 2016

THESIS SUBMITTED IN PARTIAL FULFILLMENT OF
THE REQUIREMENTS FOR THE DEGREE OF

MASTER OF SCIENCE

in

THE FACULTY OF GRADUATE AND POSTDOCTORAL STUDIES
(Zoology)

THE UNIVERSITY OF BRITISH COLUMBIA
(Vancouver)

January 2020

The following individuals certify that they have read, and recommend to the Faculty of Graduate and Postdoctoral Studies for acceptance, the dissertation entitled:

Role of Wnt signaling in asymmetric neurite pruning in *Caenorhabditis elegans*

submitted by Menghao Lu in partial fulfillment of the requirements for

the degree of Master of Science

in Zoology

Examining Committee:

Kota Mizumoto, Zoology
Supervisor

Donald G. Moerman, Zoology
Supervisory Committee Member

Additional Supervisory Committee Members:

Michael Gordon, Zoology
Supervisory Committee Member

Abstract

Developmental neurite pruning is a phenomenon widely observed in different organisms including humans. Through this process, neurons selectively remove exuberant neurites by pruning to form a proper neurocircuit. Some neurites are pruned base on the competition of neuronal input, while others undergo stereotyped pruning which is controlled by morphogenic cues.

We found that in *Caenorhabditis elegans*, a cholinergic motor neuron, PDB, undergoes stereotyped neurite pruning. During PDB development, we observed two posterior branches that are stereotypically pruned. Time-lapse imaging showed that these posterior branches are retracted while the anterior branch is extending. We also found a posteriorly expressed Wnt, LIN-44, and its receptor LIN-17/Frizzled (Fz) are responsible for the pruning of the posterior neurites. In *lin-44* and *lin-17* mutant animals, the posterior neurites often failed to be pruned. Furthermore, we discovered that the activation of LIN-44/Wnt is gradient independent, and membrane-tethered *lin-44* is sufficient to induce asymmetrical posterior neurite pruning. LIN-17 and its downstream DSH-1/Dishevelled (Dsh/Dvl) proteins are recruited to the posterior neurites while either wildtype or membrane-tethered *lin-44* is expressed. Our results showed a novel contact-dependent role of Wnt in asymmetric neurite pruning.

Lay Summary

During development, our nervous system undergoes a process called neurite pruning, which will “trim” the neuronal network with high precision and shape it to the mature form. Faulty neurite pruning may contribute to neuropathic symptoms such as schizophrenia and Alzheimer’s disease. However, due to the lack of good models, genetic factors initiating this pruning process are largely unknown. This study describes a neuron in *C. elegans* with neurite pruning activity, and also reveals that Wnt, an evolutionally conserved signaling pathway, initiates neurite pruning in this neuron. The results from this study can be used to conduct further investigation into the mechanisms behind this neurite pruning, and may ultimately contribute to the understanding of nervous system development.

Preface

This work was conducted at the University of British Columbia, Life Science Institute by Menghao Lu and Dr. Kota Mizumoto. A version of this material has been published on December 5, 2019 as Lu M, Mizumoto K. 2019. Gradient-independent Wnt signaling instructs asymmetric neurite pruning in C. elegans. Elife 8:1–23. doi:10.7554/eLife.50583. I provided formal analysis, validation, investigation, visualization, methodology for all sections. Kota Mizumoto and I conceived the experiments, and wrote the manuscript together for the publication.

Table of Contents

List of Tables

List of Figures

Lists of Abbreviations

BDM	2, 3-butanedionemonoxime
cDNA	complementary DNA
C. elegans	Caenorhabditis elegans
CRD	cysteine-rich domain
Da	Dendritic arborization
GFP	Green Fluorescent Protein
Hyp	Hypodermal cell
IPB	infrapyramidal bundle
L1	Larvae stage 1
L2	Larvae stage 2
L3	Larvae stage 3
L4	Larvae stage 4
LEF	Lymphoid enhancer factor
mScarlet	red fluorescent protein mScarlet
MB	Mushroom bodies
NGM	Nematode growth medium
NMJ	Neuromuscular junction

PCR	Polymerase Chain Reaction
PCP	Planar cell polarity
SEM	Standard errors of mean
SEP	Standard error of the proportion
TCF	T-cell factor
VGCC	Voltage-gated calcium channel

Acknowledgements

First and foremost, I am grateful to have Dr. Kota Mizumoto supporting me all the time, earnestly guiding me through this study, and mentoring me with extreme patience. Sincerely, thank you for pushing me to think independently as a scientist, sculpturing my naïve thoughts, and giving me a hand when I run out of ideas. Your ingenious thought and hardworking inspire everyone to progress. I also thank the past and current lab members: Kelly, thank you for patiently explain unfamiliar things to me when I first joined our lab; Ardalan, thank you for kindly provide help whenever it is needed; Ethan, thank you for your enthusiasm in life and work; and Mizuki, thank you for sharing constructive thoughts in our experiments. It has been a great pleasure to work with such nice colleagues and friends.

Many thanks to Dr. Michael Gordon and Dr. Don Moerman, my supervisory committee members, for your suggestions during committee meetings, helping with time management of my experiments, and editing this thesis. Thanks to the reviewers from eLife, who have recognized our work, provided valuable suggestions during the revision process, and helped us to solidify our arguments. In addition, thanks to my friend Alfred, who helped me with proof reading and grammar editing.

Last but not least, I would also like to thank all the members from the Moerman's lab, not only for sharing equipment and strains with us, but also for their generous sharing of knowledge. As experts in worm genetics, they taught me a lot of things, from basic genetic lessons to useful bench tricks. I want to specifically thank Erica for helping me with whole genome sequencing sample preparation.

1. Introduction

1.1 Developmental neurite pruning

The human nervous system consists of billions of neurons that are organized into an intricate yet dynamic network. The soma of neurons is usually compact together forming nuclei, and the cell membrane forms long protrusions called axon and dendrites, collectively referred to as neurites. Those protrusions can extend far away from the soma, form synapses with certain targets, and conduct electrical or chemical signals. During embryonic and early postnatal development, the robust outgrowth of the nervous system results in over-exuberant neuronal connections, which will be gradually trimmed during the developmental stage, to generate a mature nervous system (Kantor and Kolodkin, 2003; Luo and O'Leary, 2005). The trimming of certain neurites, such as segments of axon and dendrites, without eliminating the whole neuron is referred to as neurite pruning (Low et al., 2008). Human and rodent models revealed a relationship between faulty neurite pruning and some mental disorders. In schizophrenia patients, the size of the corpus callosum is usually downsized for 0.5-1cm, suggesting an exaggerated neurite pruning (Innocenti et al., 2003). On the other hand, autistic disorders are thought to be related to macrocephaly, a symptom resulting from synaptic pruning defects (McCaffery and Deutsch, 2005). In Alzheimer's disease (AD), neuronal inflammation and microglia cell activation, hallmarks of neuronal degeneration, are often observed in the brains, which is suspected to be caused by reactivation of pruning activity (González-Scarano and Baltuch, 2002). In autism spectrum disorder (ASD), hypo- and hyper-connectivity in the brain disrupt the excitation-inhibition balance, causing high regional neural activity. On the other hand, the size of gray matter also changes (decreases in the amygdala-hippocampus and increases in frontal gyrus) in ASD patients (Mataix-Cols et al., 2011; Supekar et al., 2013).

There are two opposing mechanisms for neurite pruning, one is the activity-dependent model, in which the difference in neuronal activity between the competing axons is the driving force causing neurite pruning in one but not the other neurite. For example, between the two axons innervating the trapezius muscle in a newborn mouse, the one with weaker synaptic activity is selectively pruned (Colman et al., 1997). The other mechanism is activity independent, first proposed by Roger Sperry in in the 1950s (Meyer, 1998), whereby the decision of pruning is based on the topographical expression of certain signaling cues. A few examples from both vertebrates and invertebrates will be further discussed in the following section. Interestingly, these two types of pruning are not always mutually independent. For example in the developing mouse visual system, both Ephrin-As and neural activity in the retina work together to form proper neuronal structures along the N-T axis (Cang et al., 2008; Pfeiffenberger et al., 2006).

1.1.1 Neurite pruning in mouse hippocampus

The hippocampal mossy fiber axons in the infrapyramidal bundle (IPB) arise from granule cells in the dentate gyrus, and initially extend into hippocampal CA3 pyramidal cells at early postnatal stage (P10). In adult mice (after P45), however, IPB axons are pruned all the way back to the dentate gyrus. Previous works have shown that Semaphorin-Plexin signaling and Ephrin-Eph signaling induce the pruning of IPB. At the age of P25 and P70 respectively, *Ephb3* and *Sema3F*, are expressed in the hippocampus, selectively around the putative IPB pruning region, and their receptors *Neurophilin-2, Plexin-A3*, and *Ephrin-B3 (EFNB3)* are expressed in IBP. In *Neurophilin-2, Plexin-A3* and *Efnb3* mutant mice, IPB is significantly longer at the adult stage, suggesting a defective neurite pruning (Bagri et al., 2003; Chen et al., 2000; Xu and Henkemeyer, 2009). Cultured hippocampal neurons from the *Efnb3−/−* null mice still respond to

Semaphorin, suggesting that Semaphorin and Ephrin pathways function independently in IPB prning (Xu and Henkemeyer, 2009).

1.1.2 Neurite pruning in the *Drosophila* mushroom body

The mushroom bodies (MBs) are structures in *Drosophila* brain that function in olfaction and memory. The early-born (γ) neurons have preliminary branches both in their axons and dendrites, which are pruned during metamorphosis at the pupa stage (Lee et al., 1999). Forward genetic screenings of mutants with neurite pruning defects in γ neuron have revealed the TGF-β/EcR-B1 signaling cascade plays a role in γ neuron pruning. TGF-β ligand Myoglianin (Myo) is secreted from glia and astrocyte cells wrapping around γ neuron, and it is recognized by the receptor Baboon (Babo) on γ neuron, and activates downstream component dSmad2. Nuclear receptor Ecdysone Receptor-B1 (EcR-B1) is activated, however, the mechanism of EcR-B1 activation and its initiation of neurite pruning remain unknown (Lee et al., 2000; Yu et al., 2013; Zheng et al., 2003).

1.1.3 Neurite pruning in *Drosophila* dendritic arborization neuron

Dendritic arborization (da) neurons are sensory neurons with rigorously tiled dendrites on the body wall, and are classified into 4 morphological subtypes (Class I-IV) (Grueber et al., 2003). Researchers found that Class IV neurons undergo dendritic pruning during early metamorphosis. The larval dendrites are pruned via local degeneration, where the dendritic branches are detached from the main arbor and undergo fragmentation (Williams and Truman, 2005). The detachment is initiated by the microtubule-severing protein, Katanin (Lee et al., 2009). Local calcium surge caused by voltage-gated Ca^{2+} channels (VGCCs) at the putative pruning dendrites is observed,

and believed to trigger the fragmentation of those dendrites (Kanamori et al., 2013), however the most upstream cues that trigger neurite pruning remain elusive.

1.1.4 Neurite pruning in *C. elegans* AIM neurons

AIML and AIMR are a pair of ring interneurons located at the head region of a worm. During embryonic development, each AIM neuron extends two neurites: one anteriorly to join the nerve ring, and one cross-sectionally towards the other AIM. During the first larval stage (L1), the cross-section neurites are pruned, while the other anterior neurite is not affected. Researchers have found Wnt (CWN-1 and CWN-2) and Ror kinase (CAM-1) may play a trophic role to inhibit neurite pruning. AIM neurite pruning is hampered when Wnt-Ror kinase signaling is upregulated, while knocking out Wnts can rescue the pruning defect caused by *mbr-1(lf)*, a transcription factor that promotes neurite elimination. (Hayashi et al., 2009).

1.2 *C. elegans* as a model for studying neurite pruning

C. elegans is a free-living nematode that can be found in many different places around the world. After Sydney Brenner did original studies using *C. elegans* as a model organism (Brenner, 1974), it has become one of the most popular genetic model organisms in various research fields including neuroscience. It has a long list of advantages as a tool for genetic study, including its small size, easy (and inexpensive) maintenance, and short life cycle. Its invariable cell lineage has been described (Sulston et al., 1983; Sulston and Horvitz, 1977).

Aside from the advantages listed above, several characteristics make *C. elegans* an ideal model for studying neuronal development. First, it has a simple nervous system consisting of 302 neurons (White et al., 1986). Despite the simplicity of the *C. elegans* nervous system, the biological processes underlying neuronal development are highly conserved between *C. elegans*

and mammals. Second, combinations of fluorescent proteins and a series of tissue-specific promoters allow researchers to visualize individual neurons in live worms. Last but not least, the nervous system is not essential for the survival of the worms under laboratory condition. Therefore, we can examine the roles of genes that are essential for neurodevelopment, whose mutants are likely lethal in other organism systems.

1.3 Wnt and nervous system

1.3.1 Introduction of Wnt

In the 1980s, researchers found a region of the mouse genome susceptible to the proviral insertion of mouse mammary tumor virus, and within this region, they identified a new oncogene *int-1* (integration 1) (Nusse and Varmus, 1982). *int-1* was found to be homologous to a *Drosophila* gene *Wingless (Wg)*, which is crucial for normal wing disk development (Babu, 1977). Wnt homologs are also widely found in both vertebrates and invertebrates, including *C. elegans* (Nusse and Varmus, 1992).

Wnt proteins are secreted glycoproteins that function as gradient morphogens (Miller, 2002). A conserved cysteine is post-translationally modified with palmitate by PORCN (porcupine), which is crucial for Wnt's biological activity (Willert et al., 2003). Wnt ligand is recognized by a 7-pass-transmembrane receptor, Frizzled (Fz). Fz receptor contains a cysteine-rich domain (CRD) at the extracellular region, which will recognize and bind to Wnt. The intracellular cytoplasmic tail of the Fz receptor contains a conserved PDZ domain binding motif, and recruits Dishvelled (Dsh) when activated (Wong et al., 2003). Dsh is a cytoplasmic multidomain protein with DIX, DEP and PDZ domains. The recruitment of Dsh can activate discrete downstream

pathways: β-catenin dependent canonical pathway and two β-catenin independent non-canonical pathways.

1.3.2 Wnt signaling pathways

The canonical Wnt/β-catenin signaling pathway induces gene expression via activating the transcription factor TCF (T cell factor) by the transcriptional co-activator, β-catenin. In the absence of Wnt, a destruction complex consisting of Axin, APC, CK1 and GSK3beta phosphorylates β-catenin, and leads it to ubiquitin-dependent protein degradation. Upon Wnt exposure, the cell recognizes Wnt through Fz and its co-receptor LDL-receptor related protein (LRP), and activates Dsh to inhibit the destruction complex (Tamai et al., 2000). Then β-catenin is stabilized, brought to the nucleus to form a complex with TCF, and activate the target gene expression (Jackson and Eisenmann, 2012).

The non-canonical Wnt pathways include the planar cell polarity (PCP) pathway and the calcium pathway. The PCP pathway was first discovered in epidermal hair patterning in *Drosophila*, where it is required to establish the correct direction of those hairs (Adler, 2002). In addition to the Frizzled, the 4-pass-transmembrane protein Van Gogh (Vangl) (Wolff and Rubin, 1998), the tyrosine kinase related protein (Ryk, also called Derialed/DRL) (Yoshikawa et al., 2003), and the cadherin-like protein Flamingo (Fmi, also called Starry night/Stan) (Usui et al., 1999) are required. In general, when the PCP pathway is activated, Fz-Dsh complex localizes on one side of the cell, and Vangl and Ryk will localize on the other side. The complementary localization between Fz and Vangl is mediated by the mutual inhibition between the Dsh and Prickled which are the cytoplasmic proteins that interact with Fz and Vang, respectively (Tree et al., 2002; Usui et al., 1999; Yoshikawa et al., 2003). On top of the intracellular antagonism, Fz and Vang stabilize each other by extracellular interaction (Struhl et al., 2012). The downstream

of the PCP pathway depends on the context, including Rho subfamily, Rho-assisted kinase, mitogen-activated protein kinase (MAPK), and JNK signaling (Yang et al., 2016).

The other non-canonical Wnt pathway is the Wnt/calcium pathway. It was first recognized in the zebrafish embryo, where the researchers observed Calcium transient after inducing *Wnt5a* expression (Diane C. Slusarski et al., 1997). Calcium serves as a second messenger and activate calcium/calmodulin-dependent protein kinase II (CamKII), protein kinase C (Diane C. Slusarski et al., 1997). Calpain is also reported to be downstream of *Wnt5a* during *Xenopus* gastrulation (Zanardelli et al., 2013).

1.3.3 Secretion and transport of Wnt ligands

During development, Wnts are secreted from the Wnt-producing cells and function as gradient morphogenic cues (Bänziger et al., 2006; Strigini and Cohen, 2000). After being palmitoylated in the endoplasmic reticulum (ER) (Herr and Basler, 2012; Yu et al., 2014), Wnt binds to Wntless (Wls), which will assist in transporting Wnt to Golgi for further modification, and transportation from the Golgi to the cell surface (Bänziger et al., 2006; Moti et al., 2019).

How Wnt travels to the target cells are still under debate. Traditionally it was believed that Wnt ligands are secreted into the extracellular environment through exocytosis, and thereby travels through free dispersal. This hypothesis has been proven by different studies from *C. elegans* and *Drosophila* (Cadigan et al., 1998; Coudreuse, 2006; Klassen and Shen, 2007; Maro et al., 2009; Mizumoto and Shen, 2013; Pani and Goldstein, 2018), and direct visualization of the ligand distribution further confirmed the existence of Wnt gradient (Pani and Goldstein, 2018). However, the palmitoylation ought to make the molecule highly hydrophobic, therefore its long-range free distribution in the hydrophilic extracellular matrix is illogical. Several lines of

experiments also suggest the existence of gradient-independent Wnt signaling. For example, in *Drosophila*, both wildtype Wnt and a non-diffusible Wnt (Nrg-wg), which is a fusion protein between type-II transmembrane protein, neurotactin, and Wnt, can induce naked cuticle formation in the embryo (Zecca et al., 1996). Furthermore, another *Drosophila* study suggests that non-diffusible Wnt can induce normal wing imaginal disc formation, which has previously been believed to be regulated by the gradient distribution of Wnt (Alexandre et al., 2014). Nevertheless, there are also several models proposed for the formation of long-range Wnt signaling without free dispersion, such as extracellular vesicles (Gross et al., 2012), filopodia protrusion (Stanganello et al., 2015), and cell migration (Serralbo and Marcelle, 2014).

1.4 Wnt functions in the nervous system

In the nervous system of different organisms, Wnt signaling is reported to have crucial functions in axon guidance and synaptogenesis (He et al., 2018). For example, Wnt4 attracts axons during the midline crossing in the mouse dorsal spinal cord, through its receptor Fz3 (Lyuksyutova et al., 2003). Wnt5 is found to mediate midline crossing in *Drosophila* by repelling the axon through Fz2 and RYK (Yoshikawa et al., 2003). Wnt7a is found to induce mouse Mossy Fiber axon remodeling, changing microtubule organization, and increase synapsis formation through Fz5 and GSK3 (Hall et al., 2000; Sahores et al., 2010). During early postnatal mouse hippocampal development, Wnt7a, and Wnt7b increase synapse formation through the canonical pathway, while Wnt5a inhibits synapse formation, independent of β-catenin (Davis et al., 2008; Sahores et al., 2010). In *Drosophila*, ventral muscle M13 inhibits synapse formation from MN12 neurons, by secreting DWnt4 (Inaki et al., 2007). Alternatively, another *Drosophila* Wnt Wg is reported to be secreted from glia cells around the synaptic boutons, and promotes the development of NMJ through DFz2 (Kerr et al., 2014; Packard et al., 2002). An interesting study

on *Drosophila* serotonergic neuron (CSDn) suggests Wnt may also be required in the refining of its dendritic structure during the pupal stage, together with glutamate receptors (A. P. Singh et al., 2010).

A study found decreasing Wnt signaling by injecting Wnt antagonist Dickkopf1 into mouse amygdala specifically impairs long-term fear memory formation (Maguschak and Ressler, 2011), suggesting the importance of Wnt in the postnatal nervous system. Wnt signaling is also thought to be associated with AD and schizophrenia (Arnés and Casas Tintó, 2017; Inestrosa et al., 2012). In the case of neurodegeneration in AD, evidence suggests the disruption of Dickkopf1 and Wnt balance may be involved (Buechler and Salinas, 2018; Caricasole, 2004; Hernandez et al., 2012), and the activity of canonical Wnt signaling is abnormally down-regulated in the AD brains (Folke et al., 2018). Wnt is also implicated in schizophrenia: human Frizzled-3 (FZD3) is genetically linked to schizophrenia in a group of Japanese patients (Katsu et al., 2003), and one of the first identified risk genes disrupted in schizophrenia-1 (DISC1) is reported to interrupt Wnt signaling through altering GSK3β (K. K. Singh et al., 2010).

1.5 Wnt signaling in *C. elegans* neurodevelopment

In *C. elegans*, there are five Wnts (*egl-20, lin-44, cwn-1, cwn-2, mom-2*) and four Frizzled receptors (*mig-1, lin-17, cfz-2, mom-1*). Similar to other organisms, in the *C. elegans* nervous system, Wnt signaling controls synaptic patterning, and guides neurite outgrowth.

EGL-20/Wnt serves as a repulsive cue for the anterior outgrowth of the PVM mechanosensory neurons through two redundant receptors MIG-1 and MOM-5. In the mutants for those genes, the anterior process of PVM is either short or misguided posteriorly (Pan et al., 2006).

The other mechanosensory neurons PLMs usually project a long neurite from the cell body anteriorly and a short neurite posteriorly. This polarity is mediated by *lin-44*/wnt and *lin-17/fz*. Perturbing Wnt signaling will result in an overshooting of the posterior neurite with a shorter anterior neurite (Hilliard and Bargmann, 2006).

The oxygen sensory neuron PQR usually has a long axon extending anteriorly, and a short dendrite protruding posteriorly. LIN-44/Wnt and EGL-20/Wnt cooperatively direct the outgrowth of the PQR dendrite, where LIN-44 attracts and EGL-20 repels the dendrite outgrowth, through LIN-17/Fz (Kirszenblat et al., 2011).

In the D-type motor neuron, DD6, LIN-44 gradient from the posterior end of the worm repels the DD6 axon through LIN-17/Fz. In the *lin-44* mutants, DD6 axon overextends posteriorly, while ectopic anterior expression LIN-44 results in underextension of the DD6 axon (Maro et al., 2009).

DA8 and DA9 are two cholinergic motor neurons, whose cell bodies reside at the ventral nerve cord, send long axons anteriorly on the dorsal nerve cord along each other, and form synapses within a certain region side by side. The posterior boundaries of their synaptic regions are regulated by EGL-20 and LIN-44, with receptors MIG-1 and LIN-17, respectively (Klassen and Shen, 2007; Mizumoto and Shen, 2013).

The synapse formation of AIY, the amphid interneurons in the head region, is controlled by the canonical Wnt signaling pathway mediated by CWN-2/Wnt and CFZ-2/Fz. The large bouton at zone 2 will undergo fragmentation when Wnt signaling is knocked down, suggesting a function of Wnt in synaptic clustering (Shi et al., 2018).

1.6 The PDB neuron as a model to study neurite pruning

PDB is a cholinergic motor neuron located in the tail ganglia, derives post-embryonically from P12, one of the ventral cord precursor cells (Jiang and Sternberg, 1998). Little is known about its biological function, although a prediction using a mathematical model and the knowledge of the connectome suggests PDB is a crucial control neuron, and PDB-ablated animals display impaired ventral omega turn (in which the worm makes a sharp Ω-shape and swims backwards) (Walker et al., 2017). During a study of the Kallmann syndrome gene kal-1, H. Bulow et al. found *Pkal-1::gfp* reporter is expressed in PDB (Bülow et al., 2002), but the development of PDB has not been carefully studied.

What attracted us initially to this neuron is the astounding shape of the PDB neurite. At L4 stage, PDB presents a dramatic V-shaped neurite structure that does not exist in any other neurons. A single neurite grows from the cell body posteriorly along the ventral body wall, bends approximately 340 degrees around the tail tip, extends anteriorly along the dorsal body wall, and eventually joins the dorsal nerve cord. The question that immediately interested us was: how does PDB form this "bizarre" sharp turn?

Due to the advantage of being a post-embryonically formed neuron (Sulston and Horvitz, 1977), the development of PDB can be partially visualized using a fluorescent marker expressed under the *kal-1* promoter (Bülow et al., 2002). In this study, we found that in wildtype animals, PDB forms two stereotyped posterior branches and one anterior branch, and forms an H-shaped primeval structure during its development. The posterior branches are later pruned, while the anterior branch continues extending, and eventually matures to the V-shaped structure in adult animals. The pruning of posterior neurites is mediated by gradient-independent LIN-44/Wnt and its receptor LIN-17/Fz.

2. Materials and Methods

2.1 Nematode strain culture

2.1.1 General maintenance

All strains were cultured in the nematode growth medium (NGM) as described previously (Brenner, 1974). Bristol N2 strain was used as a wildtype reference. Maintenance is performed using stereomicroscopes (ZEISS Stemi 305 and ZEISS SteREO Discovery.V8). Unless particularly noted, all strains were grown at room temperature (~22°C) for analysis. Mutant strains used in this study are listed in Table 1.

2.1.2 Lysis of *C. elegans*

In order to expose genomic DNA from live *C. elegans*, lysis was performed prior to further molecular works. A starved plate was washed with 100μL M9 buffer, then worms and eggs were collected together with M9, and pipetted into an empty PCR tube. The supernatant was removed after quiescence, and 20μL of lysis buffer (composition listed below) was added to the pellet. The mixture was vortexed, incubated at 65°C for 1.5 hours, and 95°C for 15 minutes, in order to inactivate the proteinase.

1M KCL	2.5 mL
1M TRIS (PH=8.3)	0.5 mL
0.5M $MGCL_2$	0.25 mL
4.5% NP-40	5 mL
20% TWEEN-20	1.125 mL
0.1% GELATIN	5 mL
PROTEINASE K	Up to 60 μg/mL

MUTANT ALLELE	DISCRIPTION
lin-44(n1792)	Wnt ligand
egl-20(n585)	Wnt ligand
lin-17(n671)	Frizzled
mig-1(e1787)	Frizzled
dsh-1(ok1445)	Dishevelled
mig-5(tm2639)	Dishevelled
bar-1(ga80)	β-catenin
cam-1(gm122)	ROR1/Ryk
fmi-1(tm306)	Flamingo
vang-1(ok1142)	Vangl
unc-13(e450)	Munc13
kal-1(ok1056)	ANOS1
unc-53(e2432)	NAV1
unc-2(e55)	VGCC α1
nca-2(gk5)	VGCC α1
egl-19(n582)	VGCC α1
egl-19(n582ad952)	VGCC α1
unc-77(gk9)	VGCC α1
unc-36(e251)	VGCC α2
clp-1(tm690)	Calpain 9
clp-3(gk623576)	Calpain 3
sax-7(nj48)	L1CAM
unc-6(ce78)	Netrin
unc-6(ev400)	Netrin
unc-5(e152)	Netrin receptor
sax-3(ky123)	ROBO1
sdn-1(ok449)	Syndecan 1
eel-1(ok1575)	HECT ubiquitin ligase

Table 1. Mutants examined in this study.

2.1.3 Genotyping of strains

Some of the mutants had distinctive phenotypes, such as uncoordinated movement, multi-vulva, and egg-laying defects, which allowed us to distinguish them from wild-type animals. However, when working with mutants that were superficially wildtype, or lines with multiple genes together, those criteria were no longer reliable, therefore polymerase chain reaction (PCR) was applied to confirm the mutant genotype.

Animals were first lysed (described in section 2.1.2), and the lysis product would be used as a template for PCR amplification (DreamTaq DNA Polymerase, Thermo Fisher Scientific), with primers listed in Table 2. The genotype was then tested by electrophoresis.

2.1.4 Semi-synchronization

Animals from a healthy plate were immersed in a 1:1 mixture of household bleach (5% sodium hypochlorite solution) and 1 N NaOH for 5 min, until the body cavity was dissolved and ruptured. The fragment was washed twice by M9 buffer, and the sediment containing worm debris and eggs was pipetted back onto a fresh plate.

ALLELE NAME	PRIMER DESIGN	DIGESTION
cam-1(gm122)	aacttacactctgaagcgccgtgc ccaacttcagatgatggatcg	MseI
cca-1(gk30)	tctcgcatcctcttcctggaa gttgtttggatgcaagttctgc	
clp-1(tm690)	taccaacgagtaacggcgag taacatctggtccaagattgc	
clp-1(tm858)	cagtatgggaggtggtggtg ccaagagccaacaatctccg	
clp-3(vc40411)	ggtgttatggagcccgagttt accaaaagttgagctgccgt	DraI
dsh-1(ok1445)	cttgagatagccctgcaagac gctccaccacttgctaagattg	
egl-19(ad952)	accaatatgggtgttcgatg tcattctagctgcccatttac	MseI
egl-20(n585)	cttacctctcaaatttgaacttattcttgc cctcattaccattcaactgatag	HpyCH4V
fmi-1(tm306)	gtgaaattacatgttaactgagg tcgcctacaagaagtaacttacatg	
lin-17(n671)	ccgcatttttcgtagatcacaccg actgttgtttacagtcaattgtcattcgggtcaatt	MfeI
lin-44(miz56)	ggaaatagtgtgtggatgag aaggaaccgtggacaaccatc ccactgatcgtcgggatctc	
lin-44(n1792)	gtgcgaatcgtttgagatttcagccatg catctggttgttacacgcacaatcg	NcoI
mig-1(e1787)	acagcacaaaattcaaagccctc atttttgagccattcaaaaagaattttgaagatc	BglII
mig-5(tm2639)	aagcattcgctcctcatcatc atctcgacgatgaaacgactc	
nca-2(gk5)	agcctcaatgcaatatgggt	

	ccgcttgttcattacatgctc	
	cctgttcttcactaacattcc	
sax-7(nj48)	tgagatgaaagaaggaggagtgc	
	cacacacaatggcgcacaag	
sdn-1(ok449)	agaagtgtctcgttcagtgg	
	ctgcaaagccgacaacggtac	
	gagatgccggtcaggtgattac	
unc-36(e251)	gcagggacaattcgatttttg	HpyCH4V
	atctggacaattatcttggtgcactgg	
unc-77(gk9)	ggattgccgattgatgtttcg	
	ctgcatgtaatgatccgactg	
	ggttctatttctaccaccacc	
vang-1(ok1142)	accttgacaacgccagacag	
	gcggcaattaggcgatacctg	
	cgagcgaagtttgagtgaatc	
cwn-1(ok546)	agctggctaggtcccagaag	
	tcgaacgatcctcttcagtac	

Table 2. Genotyping primers used in this study

2.2 Transgenic lines

2.2.1 Plasmid constructs

C. elegans expression clones were made in a derivative of pPD49.26 (A. Fire), the pSM vector (a kind gift from S. McCarroll and C. I. Bargmann). *dsh-1* cDNA clone was obtained by RT-PCR from N2 mRNA using Superscript III First-strand synthesis system and Phusion High-Fidelity DNA Polymerase (Thermo Fisher Scientific). *lin-17* cDNA clone was obtained from the plasmid used in the previous work (Mizumoto and Shen, 2013).

P*kal-1::zf1-GFPnovo2-caax* plasmid The 3.7kb fragment of *kal-1* promoter was amplified from N2 genomic DNA using Phusion high fidelity enzyme (ThermoFisher Scientific, USA) and cloned into the *Sph*I and *Asc*I sites of the pSM-GFPnovo2 vector (Hendi and Mizumoto, 2018). 111bp sequence of the ZF1 zinc finger domain from *pie-1* and 51bp sequence of the CAAX sequence from human KRas were inserted into the 5' and 3' of GFPnovo2 sequence, respectively, using Gibson assembly method (Armenti et al., 2014; Gibson et al., 2009). The intestinal GFP signal was reduced by expressing *zif-1* in the intestine under the *pha-6* promoter to degrade ZF1-GFPnovo2::CAAX.

Neurotactin-BFP-lin-44 repair plasmid The plasmid containing a codon-optimized *neurotactin* cDNA with 2xHA tag was obtained from GeneArt (ThermoFisher Scientific, USA). *C. elegans* codon-optimized *BFP* with three synthetic introns was inserted into the 3' end of the Neurotactin-2xHA sequence to generate *Neurotactin-2xHA-BFP* construct. 700bp of the 5' homology arm of the *lin-44* promoter region, *Neurotactin-2xHA-BFP* (5' portion until middle of intron 1), *BFP* (3' portion from intron 1), 700bp of the 3' homology arm spanning *lin-44* coding region are cloned into the *Sac*II and *Not*I sites of a dual-marker selection cassette (*loxP* + P*myo-*

2::*GFP*::*unc-54* 3′UTR + P*rps-27*::*neoR*::*unc-54* 3′UTR + *loxP* vector) (Au et al., 2019; Gibson et al., 2009).

lin-44 gRNA constructs Two 19bp gRNA sequences (gRNA3-CGATCAGTGGTGCACCTGC, gRNA4- TATTTCCGTCTTCAGCCAA) near the start codon of the *lin-44* gene were selected using the CRISPR guide RNA selection tool (http://genome.sfu.ca/crispr/), and were cloned into *Rsa*I site of the sgRNA (F+E) vector, pTK73 (Obinata et al., 2018).

2.2.2 Creating extrachromosomal arrays by microinjection

The transgenic lines were generated using standard microinjection method (Fire, 1986; Mello et al., 1991). Needles were pulled by Model P-97 micropipette puller (Sutter Instrument, USA), and injection was operated using micromanipulator (Narishige, Japan) on an inverted microscope (Axiovert 300 from Carl Zeiss). Plasmids used in this experiment were listed in Table 3.

2.2.3 Transgenes

The transgenic lines were generated using standard microinjection method (Fire, 1986; Mello et al., 1991): mizIs9 (Pkal-1::zf1-GFPnovo2::CAAX; Pvha-6::zif-1; Pkal-1::mCherry::rab-3); wyIs486 (Pflp-13::2xGFP, Pplx-2::2xmCherry; Podr-1::RFP); mizEx248, mizEx389 (Plin-44::lin-44; Podr-1::RFP); mizEx349, mizEx350 (Plin-44::egl-20; Podr-1::RFP); mizEx384, mizEx385 (Pegl-20::lin-44, Podr-1::RFP); mizEx380, mizEx381 (Punc-129dm::lin-44, Podr-1::RFP); mizEx386, mizEx387 (Pkal-1::lin-17; Podr-1::RFP), mizEx374, mizEx376 (Prgef-1::lin-17; Podr-1::RFP); mizEx366 (Pmig-13::GFP::rab-3; Pmig-13::lin-17::mCherry; Podr-1::GFP); mizEx271 (Plin-44::BFP; Podr-1::GFP); mizEx295 (Pkal-1::lin-17::GFPnovo2; Pkal-1::bfp; Podr-1::GFP); mizEx291 (Pkal-1::dsh-1::GFPnovo2; Pkal-1::bfp; Podr-1::GFP). All

rescuing constructs were injected at 10ng/µl except Punc-129dm::lin-44 which was injected at 20ng/µl.

2.2.4 Integration of extrachromosomal arrays

The marker system (*mizIs9*) used in this experiment was integrated into the chromosome through UV radiation. A healthy non-starved plate with the desired transgenic line was treated with 40000 µJ of UV radiation. From this plate, 40 L4 animals (P0) were transferred into 20 plates, and stored under 16 °C overnight. ~400 second-generation animals (F2) from those plates are singled and screened for successful homozygous integration.

2.2.5 CRISPR-Cas9 genome editing

The repair template plasmid, two *lin-44* sgRNA plasmids and a Cas9 plasmid (Addgene# 46168) (Friedland et al., 2013) were co-injected into young adults. The candidate genome-edited animals were screened based on G418 resistance and uniform expression of P*myo-2::GFP* in the pharynx as described previously (Au et al., 2019). The selection cassette was excised by injecting Cre recombinase plasmid (pDD104, Addgene #47551). Excision of the selection cassette, which was inserted within the first intron of BFP, reconstituted *Neurotactin-2xHA-BFP-lin-44.* The junctions between *neurotactin* and *BFP* as well as *BFP* and *lin-44* coding sequences were confirmed by Sanger sequencing.

2.3 Microscopy

2.3.1. Confocal laser scanning microscopy (CLSM)

In this study, the object of interest was labeled using fluorescent proteins (described accordingly in the result session and Table 3), and observed through confocal laser scanning microscopy (Carl Zeiss LMS800). Animals were mounted on 2% agarose pads, and immobilized

using a water solution of 7.5nM levamisole (Sigma-Aldrich, USA) and 0.225 M BDM (2, 3-butanedionemonoxime) (Sigma-Aldrich, USA). The fluorescent images were taken by 63x 1.4 N.A. oil immersion lens (for animals around L2 stage) and 40x 1.4 N.A. oil immersion lens (for animals at L4 stage).

2.3.2 24h-rescue assay

After 26h under room temperature, the animals from a synchronized plate (see "2.1.4 Synchronization") were imaged by CLSM. Each worm was labeled and gently transferred into separate plates. After recovering and growing for another 24h, animals that successfully reached L4 stage were sampled again by CLSM.

2.3.3 Time-lapse CLSM

To visualize the dynamic events of PDB neurite pruning, we performed time-lapse imaging with the CLSM. Animals were carefully mounted onto 5% agarose pads, and immobilized using 1μL microbeads suspension (Alfa Aesar™ Polystyrene latex microsphere, 0.10 micron, 2.5 wt% dispersion in water, mixed with M9 buffer at 1:1 ratio). Coverslides were sealed with Vaseline (Vaseline® Jelly Original), to avoid dehydration of the animals and agarose during the imaging process. Animals are imaged by 63x lenses (1% laser power at 488nm, with a scanning speed at 0.40s/frame, each frame contains 12 Z-stacks (9.46μm/Z-stack), and an interval of 5 minutes between frames.

2.3.4 Quantification of GFP intensity

For quantification of LIN-17::GFP and DSH-1::GFP signal at the growth cones, 1.34 μm × 0.37 μm (LIN-17::GFP) or 1.54 μm × 0.46 μm region of interest (ROI) were set at the tip of anterior and posterior neurites. As an indicator of cell position, we have used cytoplasmic BFP

signal expressed by xyz promoter. The signals of the GFP and BFP channels in the region adjacent to the neurite were subtracted from those of neurite using the same size of ROI. The ratio between the GFP and BFP signals were then used as a relative indicator of GFP level.

2.4 Quantification

Confocal images were examined using ZEISS ZEN Imaging Software (blue edition). We performed quantification of PDB neurite structure at L4 stage and DD6 axon guidance using ZEISS Axioplan 2 universal microscope.

Data were processed using Prism7 (GraphPad Software, USA). We applied one-way ANOVA method for comparison among more than three parallel groups with multiple plotting points, and Chi-square test (with Yates' continuity corrected) for comparison between two binary data groups. Data were plotted with error bars representing standard errors of mean (SEM) or standard error of the proportion (SEP). *, ** and *** represent P value <0.05, <0.01 and <0.001 respectively.

3. Results

3.1 Neurite pruning happens during PDB development

3.1.1 PDB is visualized by marker system *mizIs9*

In order to visualize PDB neurite structure, we fused a membrane bound green fluorescent protein (GFPnovo2::CAAX) with 3.6kb of 5' upstream sequence of *kal-1* gene (Bindels et al., 2016; Hendi and Mizumoto, 2018). Any truncated form of this promoter region apparently will ablate its expression in PDB (Wenick and Hobert, 2004), therefore in order to reduce unwanted intestinal expression, we applied the ZF1/ZIF-1 degradation system (Armenti et al., 2014) by inserting a ZF1 zinc-finger domain before GFPnovo2, and induce ZIF-1 expression using *Pvha-6*, to specifically degrade ZF1::GFPnovo2 chimeric protein in the intestine. To visualize the synaptic structure, we also labeled a presynaptic protein RAB-3 with mCherry, by *Pkal-1::mCherry::rab-3* (Bülow et al., 2002) (see materials and methods). At L4 stage, PDB has a unipolar neurite that extends posteriorly along the ventral body wall, forms a drastic turn at the tail tip, and extends anteriorly along the dorsal body wall. This extrachromosomal array is integrated into the chromosome and named *mizIs9* (**Figure 1A**). To confirm the competition of *kal-1* promoter does not have an unexpected impact on PDB, we also examined *kal-(ok1056)*, and found PDB structure is superficially not different from wildtype.

3.1.2 Transient posterior neurites exist during PDB development

To understand the development of PDB, we examined younger worms while PDB is still growing. We performed semi-synchronization on the animals to create a population at a similar developing stage, and found PDB can be visualized as early as 26 hours post hatching (hph) (approximately L2 stage) with *mizIs9*. Surprisingly we found 26 hph animals tend to have a

unique transient structure, where one or two neurites growing posteriorly can be observed at the turning point (29/39), however only a few older animals at 50 hph (L4 stage) have any posterior neurite left (7/40) (**Figure 1B**).

To observe this phenotype in more detail, we developed a protocol named 24h-assay, to visualize the PDB structure in a single animal at both 26 hph and 50 hph (**Figure 2**). Interestingly, we found 69 branches from 43 animals at 26 hph, which are reduced to only 12 branches at 50 hph (**Figure 1C, D**).

This observation suggests that the PDB neurite may form branches twice at the tail tip during the early development of PDB: the neurite from cell body first branches vertically to create a vertical arbor (referred to as the primary branch), and slightly later, it branches again horizontally along the dorsal body wall (referred to as the secondary branch). After the two branching events it forms a temporary H-shaped structure: two neurites orienting posteriorly (referred to as the posterior branches) and one neurite orienting anteriorly (referred to as the anterior branch) (**Figure 1E**).

3.1.3 Transient posterior neurites are stereotypically pruned by retraction

Neurons could prune their neurites either by retracting or severing them. During retraction, the neurite structure is reabsorbed by the neuron without fragmentation, while severing is often followed by Wallerian degeneration, where the neurite structure is fragmented, and absorbed by surrounding cells (Schuldiner and Yaron, 2015). In order to distinguish between these two pruning mechanisms, we performed time-lapse imaging to directly visualize the pruning event. We observed that the posterior neurites become shorter over time, and did not observe

fragmentation, suggesting that the pruning of the PDB neurites is accomplished through neurite retraction (**Figure 3**).

To determine if the neurite pruning is activity dependent, we also examined *unc-13*, which encodes a munc13 homolog in *C. elegans*. This protein is required for the docking, priming, and release of synaptic vesicles. The *unc-13* mutants lose the ability of neurotransmitter release, and thereby result in severe uncoordination (Richmond et al., 1999). The structure of PDB is unaffected in *unc-13* mutants at the L4 stage (**Figure 4D**), and the trend of posterior neurite reduction from early (L2) to late larval stages (L3-L4) is seemingly not different from N2 (**Figure 1B**), suggesting neural activity is not required in PDB neurite pruning.

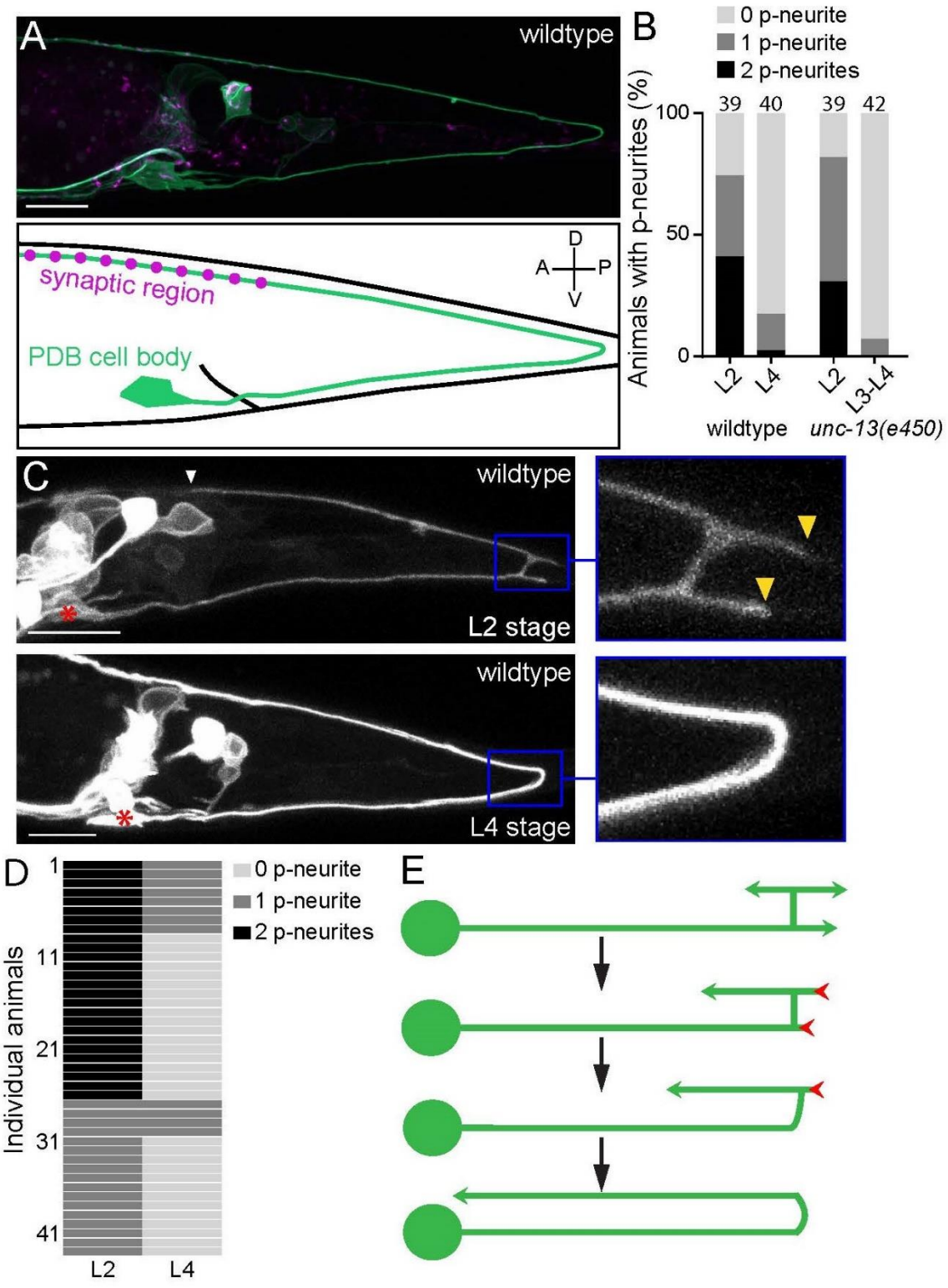
A
wildtype
synaptic region
PDB cell body
D
A
P
V
B
0 p-neurite
1 p-neurite
2 p-neurites
Animals with p-neurites (%)
100
50
0
39
40
39
42
L2
L4
L2
L3-L4
wildtype
unc-13(e450)
C
wildtype
L2 stage
wildtype
L4 stage
D
Individual animals
1
11
21
31
41
0 p-neurite
1 p-neurite
2 p-neurites
L2
L4
E

Figure 1. PDB neurites undergo stereotyped asymmetric pruning during development. (**A**) Structure of PDB labeled by the *mizIs9* transgene. The PDB process and presynaptic sites are labeled with GFPnovo2::CAAX (green) and mCherry::RAB-3 presynaptic vesicle marker (magenta), respectively. A schematic is shown in the bottom panel. (**B**) Quantification of the number of posterior neurites (p-neurites) in semi-synchronized populations of wildtype and *unc-13* mutants at L2 and L4 stages respectively. Sample number is indicated above each bar (**C**) Representative images of the posterior neurite pruning event in a wildtype animal at L2 and L4 stages. The regions of posterior neurites are magnified in the right panels. Asterisks represent the PDB cell body. White and yellow arrowheads denote the end of anterior and posterior neurites, respectively. (**D**) Quantification of the posterior neurite number of 43 wildtype animals at L2 and L4 stages. (**E**) A schematic of asymmetric neurite pruning during PDB development. Green and red arrowheads represent growing and pruning neurites. Scale bars: 10μm.

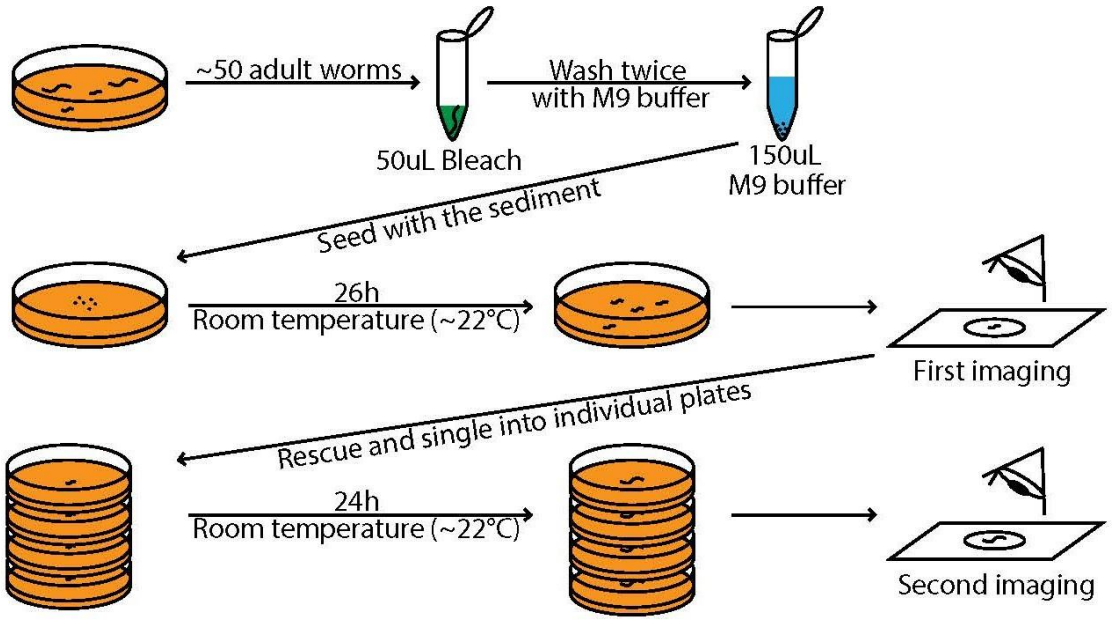

Figure 2. Schematics for 24h assay

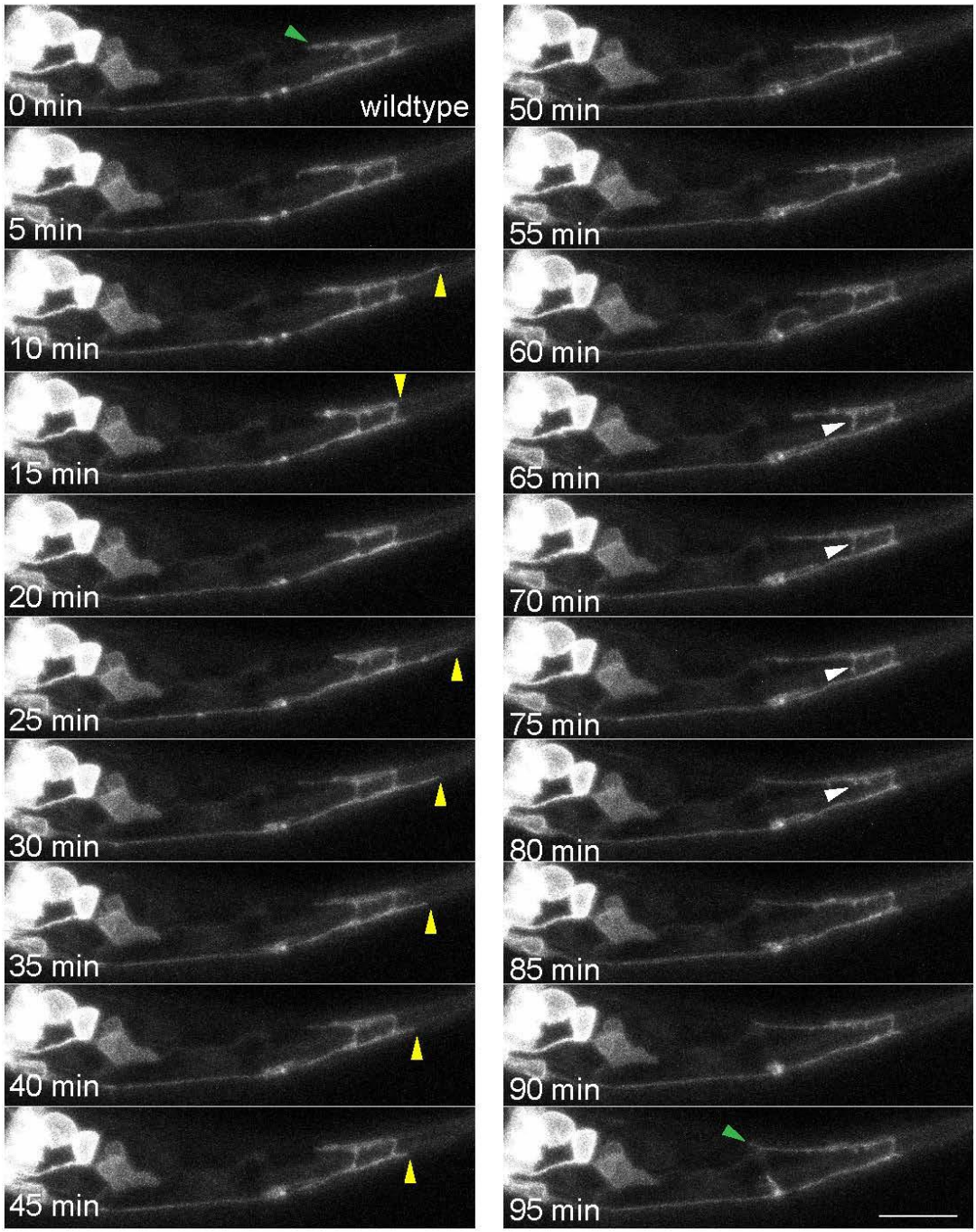
0 min
wildtype
5 min
10 min
15 min
20 min
25 min
30 min
35 min
40 min
45 min
50 min
55 min
60 min
65 min
70 min
75 min
80 min
85 min
90 min
95 min

Figure 3. Time-lapse imaging of PDB neurite pruning. PDB neurite is labeled with ZF1-GFPnovo2::CAAX of the *mizIs9* transgene. Images were taken every 5 minutes. Green arrowheads denote the end of anterior neurite in the first and last frame, and yellow arrowheads denote the end of posterior neurites during two pruning events. White arrowheads indicate transient neurites from the anterior neurites. We did not conduct detailed analyses on the pruning of these neurites since their position and the timing are less stereotyped than the posterior neurites. Scale bars: 10μm.

3.2 LIN-44/Wnt induces PDB neurite pruning through LIN-17/Fz

3.2.1 *lin-44/wnt* is required for the development of PDB

The next question we aimed to explore is the biochemical cues inducing neurite pruning of the posterior neurites in PDB. A recent study showed PDB neurite structure is disrupted in the mutants of Wnt and syndecan proteoglycans (Saied-Santiago et al., 2017). There are two Wnts secreted at close range to PDB, *lin-44* and *egl-20*, which have been reported to have pivotal roles along the anterior-posterior axis (Hilliard and Bargmann, 2006; Kirszenblat et al., 2011; Klassen and Shen, 2007; Maro et al., 2009; Mizumoto and Shen, 2013; Pan et al., 2006; Shi et al., 2018). Previous work has shown that *lin-44* is mainly expressed in the four hypodermal cells (hyp8-11) at the tail tip region around the PDB turning point (Herman et al., 1995) (**Figure 4A**). We therefore examined the relative position of those expressing cells and PDB neurites during development. Surprisingly, we found the posterior neurite often directly contacts hyp10, while the anterior neurite can extend along the isthmus between hypodermal cells and the cuticle (**Figure 4B, C**). On the other hand, *egl-20* is mainly expressed from the proctodeum region around the PDB cell body (Whangbo and Kenyon, 1999).

Then we asked whether Wnts function in PDB development, by examining the PDB neuron structure at the L4 stage in *lin-44/wnt* and *egl-20/wnt*. Due to the function of *lin-44* in the asymmetric cell division of the PDB precursor cell P12 (Jiang and Sternberg, 1998), a considerable proportion of *lin-44* animals lacked PDB. In the animals with properly differentiated PDB, *lin-44/wnt* mutants showed various defects in PDB neurite structure (**Figure 5A, B**). We first categorized them by the development of anterior neurite: animals with abnormally short or missing dorsal-anterior neurite (**Figure 5A, lower panel**), or misrouted ventral neurite are classified as "guidance defects" (24/100); animals with no visible PDB structure are classified as "linage defects" (6/100). We then categorized the rest of the animals (70 in total) by the presence or absence of posterior neurites: 38 animals with visible posterior neurites remained are classified as "p-neurites" (**Figure 5A, upper panel**), while only 32/70 of those animals had normal PDB structure. In contrast, *egl-20(n585)* animals did not have detectable defects in PDB structure (**Figure 5B**).

Next, we further examined the pruning defect in *lin-44(n1792)* mutants through 24h-rescue assay. A notable proportion of animals had defective H-shaped structure (excessive branching or mispositioned primary branch) at 26 hph. In order to be comparable, those animals were excluded from this study. Around twenty animals at 26h post hatching with wildtype-like PDB structure were carefully selected and sampled (**Figure 6A upper panel**). After 24h development, most of the *lin-44(n1792)* animals still had posterior branches retained (35/50), significantly different from N2, which indicates a defect in PDB neurite pruning (**Figure 6A lower panel, C, D**).

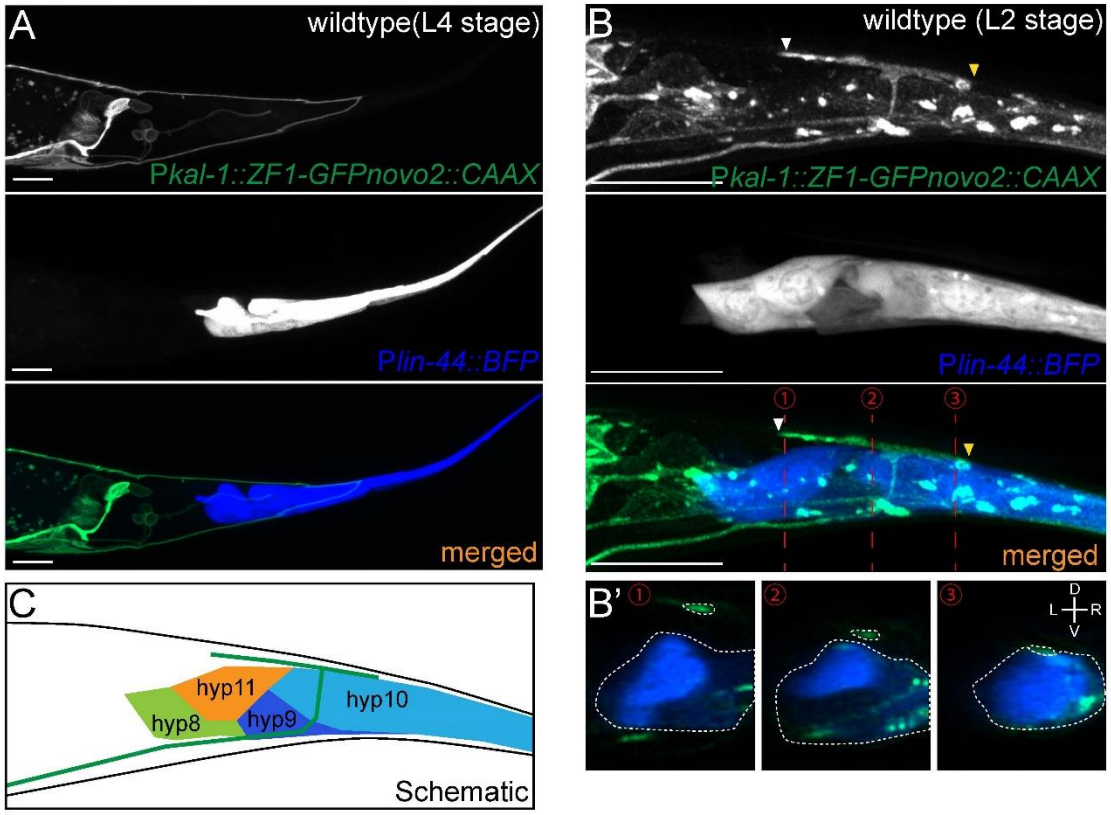

Figure 4. *lin-44/wnt* expressed adjacent to PDB posterior neurites is required for PDB development. (**A and B**) Representative images of PDB neurite labeled with *mizIs9* (top panels), *lin-44*-expressing cells labeled with P*lin-44::BFP* (middle panels) and merged images (bottom panels) at the L4 stage (**A**) and during posterior neurite pruning at the L2 stage (**B**). White and yellow arrowheads denote anterior and posterior neurites respectively. (**B'**) The transverse section of three positions of PDB neurites (indicated by red dotted lines in **B**) are reconstituted from the z-stack images shown in **B**. Dotted circles highlight PDB neurites and *lin-44*-expressing cells. (**C**) A schematic of (**B**). Green line represents PDB neurites. Scale bars: 10µm.

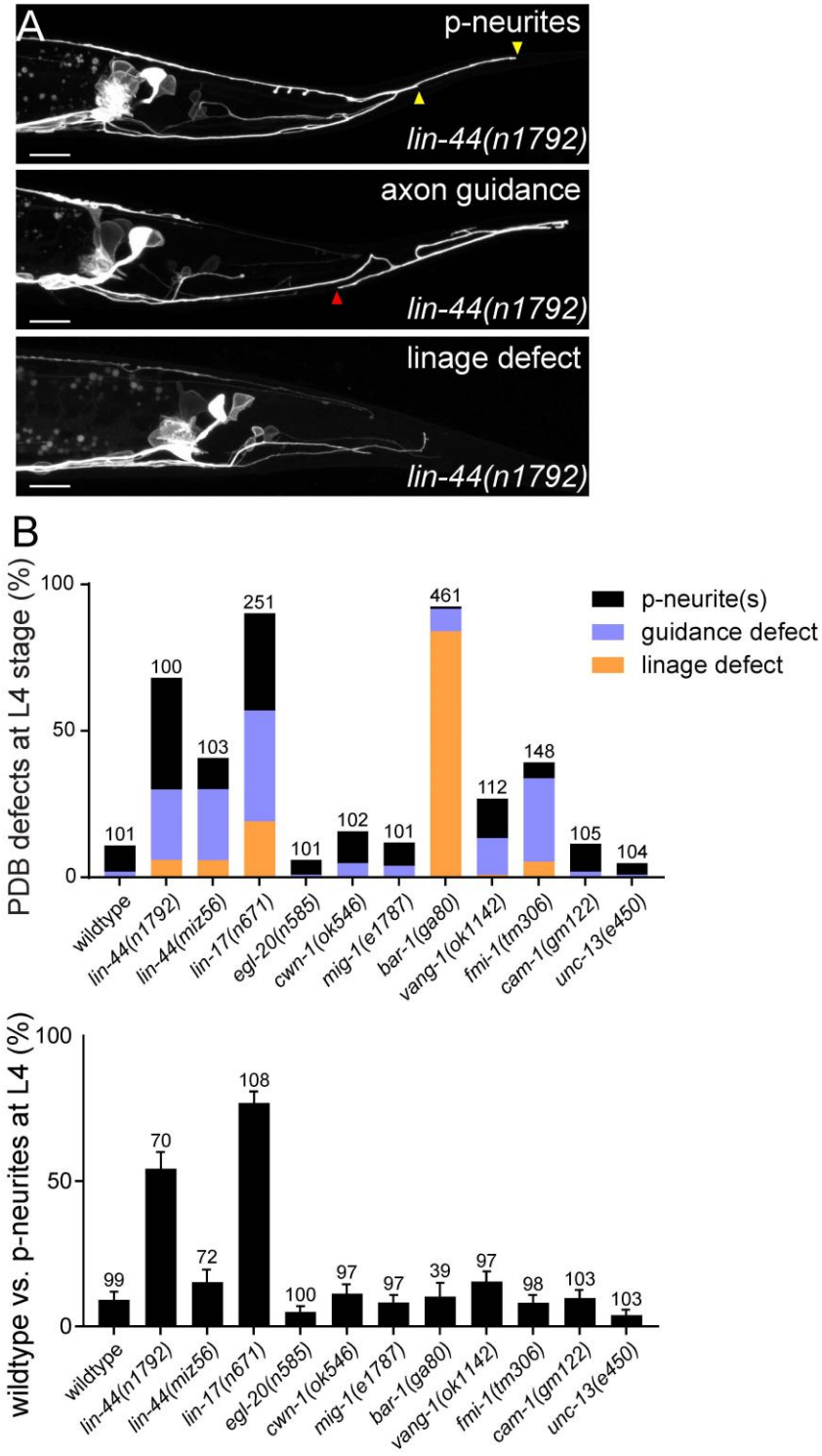
A
p-neurites
lin-44(n1792)
axon guidance
lin-44(n1792)
linage defect
lin-44(n1792)
B
PDB defects at L4 stage (%)
p-neurite(s)
guidance defect
linage defect
wildtype
lin-44(n1792)
lin-44(miz56)
lin-17(n671)
egl-20(n585)
cwn-1(ok546)
mig-1(e1787)
bar-1(ga80)
vang-1(ok1142)
fmi-1(tm306)
cam-1(gm122)
unc-13(e450)
wildtype vs. p-neurites at L4 (%)

Figure 5. Cell fate and guidance defects of PDB in the mutants of Wnt signaling components. (**A**) Representative images of PDB with posterior neurites (top panel), guidance defects (medium panel) and linage defect (bottom panel) in *lin-44* mutants. Yellow arrowheads denote posterior neurites, and red arrowhead denotes anterior neurite failed to reach the dorsal nerve cord. (**B**) Quantification of the animals with defects in PDB cell fate specification, neurite guidance neurite pruning and at L4 stage. Sample numbers are shown above each bar. Scale bars: 10μm.

3.2.2 *lin-17/fz* is the downstream receptor for *lin-44/wnt*

LIN-17 and MIG-1 are Frizzled proteins and have been reported to function as downstream receptors for LIN-44 in different contexts (Herman et al., 1995; Hilliard and Bargmann, 2006; Kirszenblat et al., 2011; Klassen and Shen, 2007). We examined null mutants of these two genes, by checking PDB structure at L4 stage. We did not find any defect in *mig-1(e1787)* mutants, while there are various defects observed in *lin-17(n671)*, including cell fate, polarity, guidance defects and also pruning defect (**Figure 5B**). To further confirm the result, we performed our 24-hour assay, and found *lin-17(n671)* mutants showed similar defects in PDB neurite pruning phenotype as *lin-44(n1792)* animals (**Figure 6B-D**). To investigate if *lin-17* functions with *lin-44* in the same signaling pathway, we also generated *lin-44(n1792); lin-17(n671)* double mutants, and found it is indifferent from single mutants, suggesting they are in the same genetic pathway (**Figure 6C, D**).

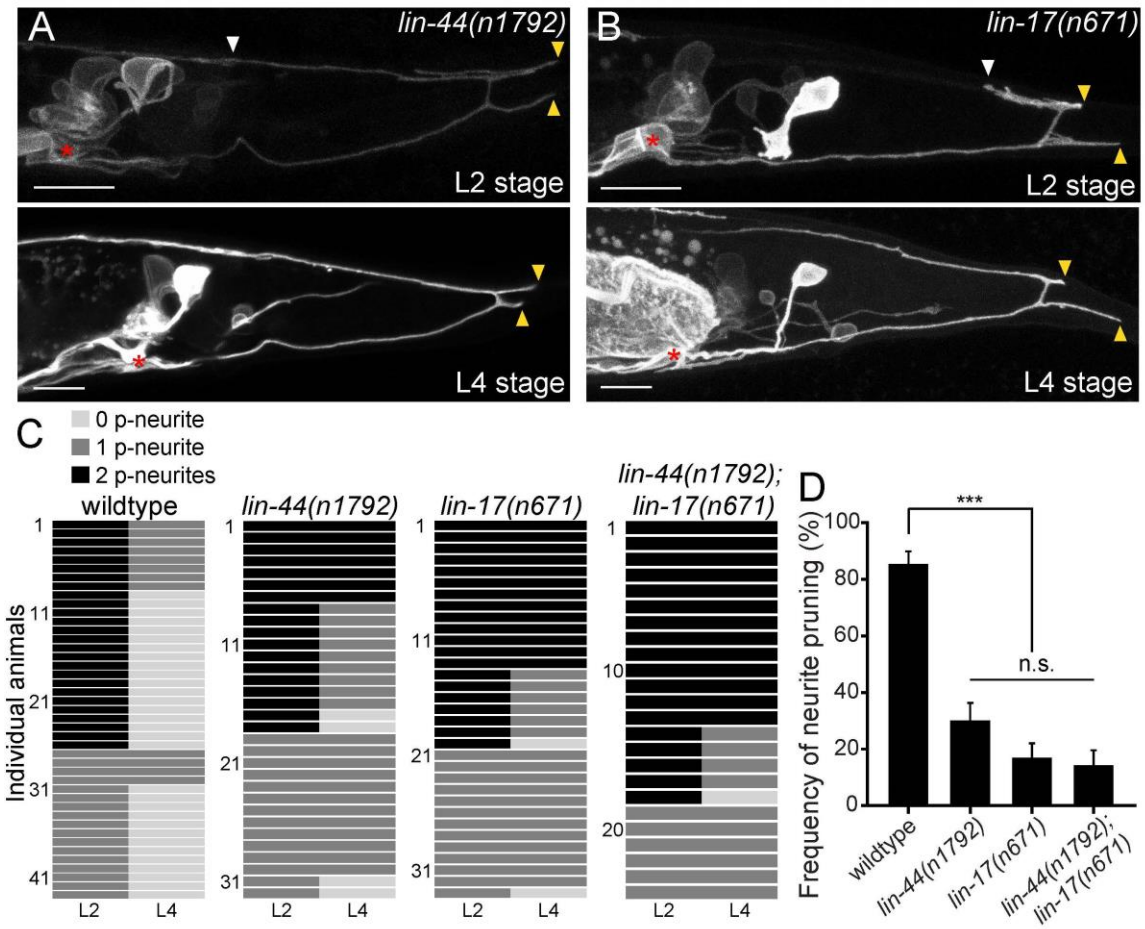

Figure 6. *lin-44/wnt* and *lin-17/fz* are required for the posterior neurite pruning.

(**A** and **B**) Representative images of single animals of *lin-44(n1792)* (**A**) and *lin-17(n671)* (**B**) mutants at L2 (top panels) and L4 (bottom panels) stages. Asterisks represent PDB cell body. White and yellow arrowheads denote anterior and posterior neurites respectively. (**C**) Quantification of the posterior neurite number of individual animals at L2 and L4 stages in each genetic background. Note that quantification of wildtype is from Figure 1. (**D**) Quantification of the posterior neurite pruning frequency. *** $p < 0.001$; n.s., not significant (Chi-square with Yates' correction). Error bars represent standard error of proportion (SEP). Scale bars: 10μm.

3.2.3 *lin-17/fz* functions cell autonomously in PDB to induce neurite pruning

To examine the cell-autonomous function of *lin-17*, we conducted tissue-specific rescue experiment. We expressed *lin-17* cDNA from the pan-neuronal promoter *Prgef-1* and the PDB promoter *Pkal-1* in *lin-17(n617)* mutants. Both pan-neuronal expression and PDB expression of *lin-17/fz* rescued the neurite pruning phenotype caused by *lin-17(n671)*, suggesting *lin-17* functions cell-autonomously in PDB to induce neurite pruning (**Figure 7A, B**). We noticed the rescue from *kal-1* promoter is not as efficient as *rgef-1* promoter, which is possibly caused by the slight late onset of *kal-1* promoter. We also checked the expression pattern of *lin*-17, by co-expressing *Plin-17::gfpnovo2* and *Pkal-1::mCherry* together in wildtype animals, and found LIN-17/Fz is expressed in many neurons including PDB (**Figure 7C)**.

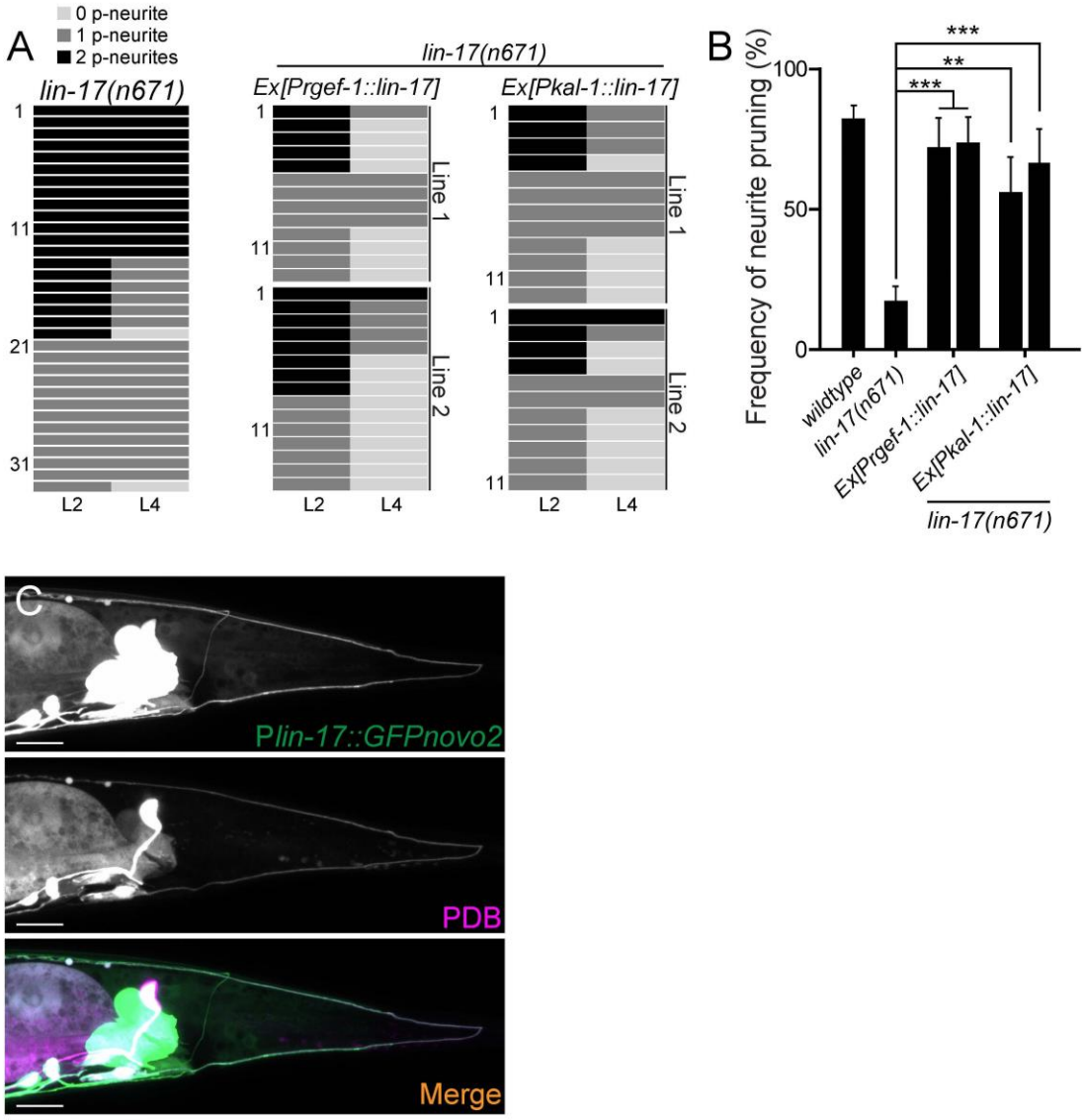

Figure 7. *lin-17/fz* acts cell-autonomously in PDB. (**A**) Quantification of the posterior neurite numbers of individual animals at L2 and L4 stages in *lin-17* mutants and *lin-17* mutants with rescuing transgenes. Note that quantification of *lin-17* mutants is from Figure 3. Two independent transgenic lines are quantified (line #1 and line #2) for each rescuing construct. (**B**) Quantification of posterior neurite pruning frequency. *** $p < 0.001$; ** $p < 0.002$ (Chi-square test with Yates' correction). Error bars represent standard error of proportion (SEP). (**C**)

Expression pattern of *lin-17* around the tail region. The PDB process is labeled with mCherry (magenta), and lin-17 expressing cells are labeled with GFPnovo2 (green). Scale bars: 10μm.

3.2.4 LIN-44/Wnt but not EGL-20/Wnt instructs PDB neurite pruning

Based on the correlation of the LIN-44 expression pattern and the pruning neurites, we hypothesized LIN-44/Wnt serves as a positional cue rather than a permissive cue to initiate PDB neurite pruning. To test this hypothesis, we expressed LIN-44 ectopically from the anterior region using *egl-20/Wnt* promoter and *unc-129dm* in *lin-44(n1792).* If LIN-44 functions as an instructive cue, anterior expression should induce normal pruning of posterior neurite. Consistently, we did not observe rescue of the neurite pruning defect in *lin-44(n1792)* from either *Ex[Pegl-20::lin-44]* or *Ex[Punc-129dm::lin-44]* (**Figure 8**), suggesting the expression of *lin-44/wnt* from the posterior end of animal is required.

In many cases EGL-20 and LIN-44 play cooperative and redundant roles (Gleason et al., 2006; Mizumoto and Shen, 2013; Yamamoto et al., 2011). We therefore tested if *egl-20/wnt* can replace the function of *lin-44/wnt* to initiate neurite pruning. However, expressing *egl-20* from *lin-44* promoter did not rescue *lin-44(lf)* phenotype either (**Figure 8**). Consistently, in the mutants of *egl-20(n585)* and its putative receptors *mig-1/fz* and *cam-1/Ror*, PDB structure is largely unaffected at L4 stage (**Figure 5B**), suggesting the function in PDB neurite pruning is *lin-44* specific. Another Wnt gene, *cwn-1*, is also expressed in the posterior region of the worm (Harterink et al., 2011). The PDB morphology was indistinguishable from wildtype in the *cwn-1* mutants (**Figure 5B**). While we do not completely exclude the involvement of other Wnts, our results indicate that LIN-44 is the major instructive cue for PDB neurite pruning.

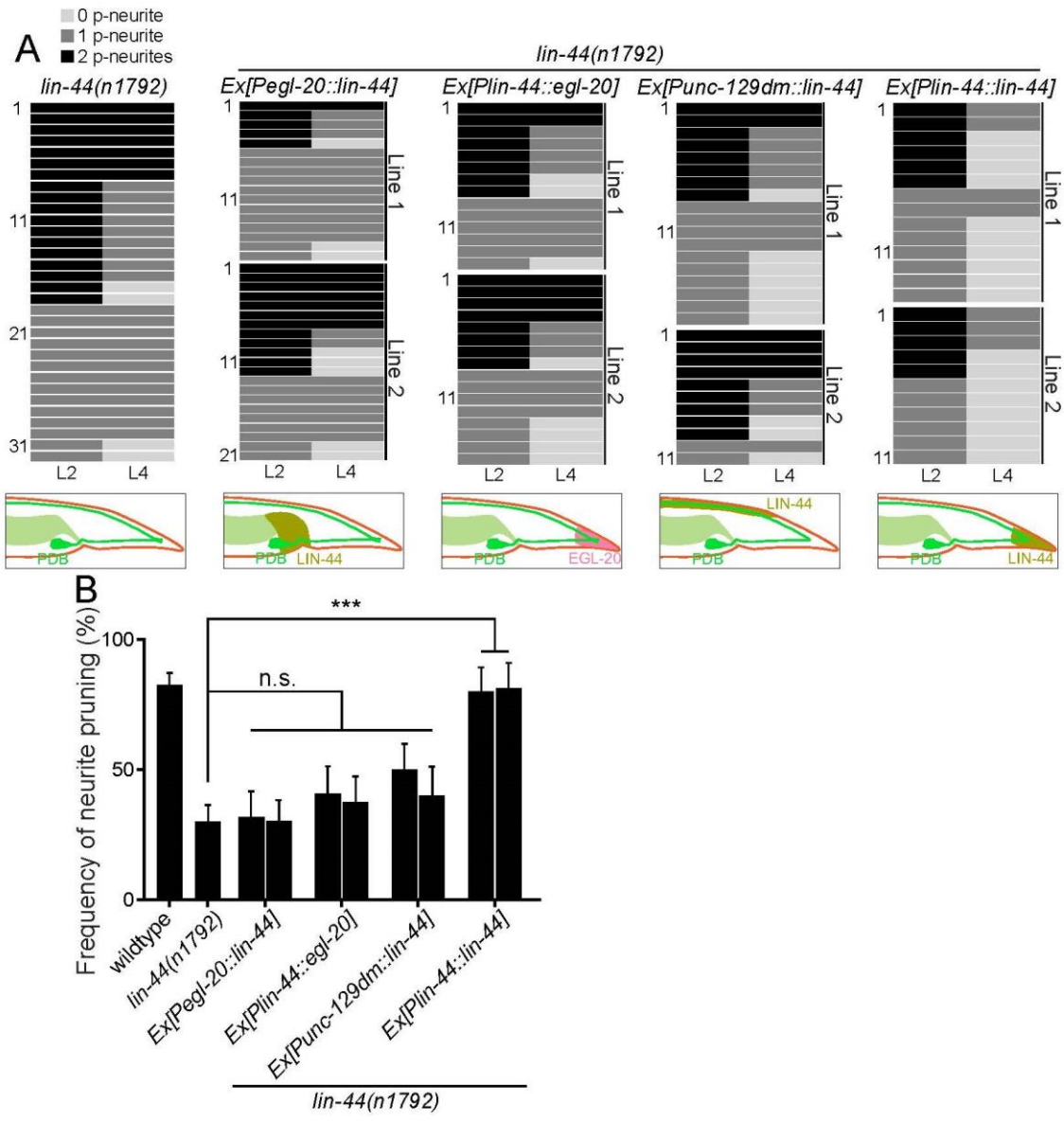

Figure 8. *lin-44* but not *egl-20* instructs neurite pruning in PDB. (**A**) Quantification of the posterior neurite numbers of individual animals at L2 and L4 stages in *lin-44* mutants and *lin-44* mutants with rescuing transgenes. Note that the quantification of *lin-44* mutants is from Figure 3. Bottom panels are schematics showing the expression domain of *lin-44* (green) and *egl-20* (magenta) in each genotype. Two independent transgenic lines are quantified (line #1 and line #2) for each rescuing construct. (**B**) Quantification of posterior neurite pruning ratio. *** p <

0.001; n.s., not significant (Chi-square with Yates' correction). Error bars represent standard error of proportion (SEP).

3.3 LIN-44/Wnt instruct PDB neurite pruning in a gradient independent manner

3.3.1 NRT-BFP-LIN-44 can instruct normal PDB neurite pruning

The V-shape of the adult PDB neurite is derived from an H-shape structure, where anterior and posterior growth cones are initially very close to each other. Super-resolution microscopy suggests the posterior neurite often directly contacts with the most posterior *lin-44* expressing cell, hyp10, while the anterior neurite and *lin-44* expressing cells are usually apart, within the level of micrometer (**Figure 2B and 2C**).

Previous studies have shown that LIN-44 functions as a gradient signal to regulate axon outgrowth in DD6, PQR, PLM neurons, and to inhibit synapse formation in the DA9 neuron (Hilliard and Bargmann, 2006; Kirszenblat et al., 2011; Maro et al., 2009; Mizumoto and Shen, 2013). How does LIN-44 induce pruning of the posterior but not the anterior neurites of PDB? One possible explanation is high concentration of LIN-44 is formed only around the expressing cells, and it is necessary to trigger neurite pruning.

To test our hypothesis, we took advantage of the membrane-tethered Wnt developed in *Drosophila* (Zecca et al., 1996). A type-II transmembrane protein Neurotactin (Nrt) is fused at the 5’ end of Wingless/Wnt, and the chimeric protein Nrt-Wg is used to examine the gradient-independent role of Wingless/Wnt, because of its inability to form long-range gradient through simple diffusion (Alexandre et al., 2014). In this study, we generated a membrane-tethered *lin-44*

allele *miz56[nrt-bfp-lin-44],* by inserting a codon-optimized Neurotactin (Nrt) and BFP into the endogenous *lin-44* locus through CRISPR (**Figure 9A**). BFP signal can only be detected on the membrane of the *lin-44*-expressing hypodermal cells, suggesting NRT-BFP-LIN-44 fusion protein is tethered to the cell membrane (**Figure 9B**). Interestingly, we observed normal neurite pruning in *nrt-bfp-lin*-44 animals (**Figure 9C-E**), suggesting the membrane-tethered LIN-44 is sufficient to induce normal neurite pruning in PDB.

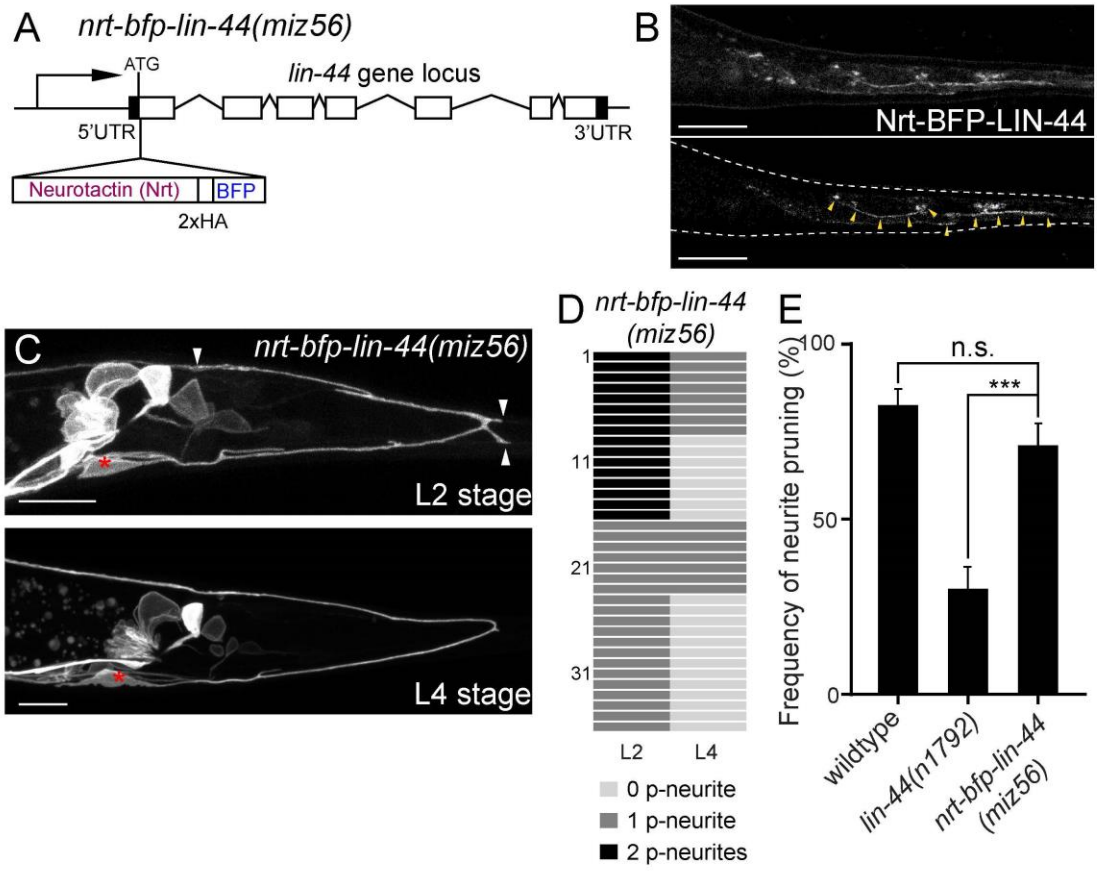

Figure 9. Membrane-tethered LIN-44 is sufficient to induce posterior neurite pruning in PDB. (**A**) A genomic structure of *lin-44* locus in *nrt-bfp-lin-44(miz56)* mutants. (**B**) Subcellular localization of Nrt-BFP-LIN-44 in the adult animal. Maximum projection (top panel) and single plane (bottom panel) from z-stack images. Arrowheads denote Nrt-BFP-LIN-44 signal on the

membrane. (**C**) Representative images of PDB structure labeled with *mizIs9* showing the pruning of posterior neurites in *nrt-bfp-lin-44(miz56)*. (**D**) Quantification of the posterior neurite numbers of 36 individual animals at L2 and L4 stages in *nrt-bfp-lin-44(miz56)* mutants. (**E**) Quantification of posterior neurite pruning frequency. *** $p < 0.001$; n.s., not significant (Chi-square with Yates' correction). Error bars represent standard error of proportion (SEP). Scale bars: 10μm.

3.3.2 NRT-BFP-LIN-44 does not function as a long range cue

Evidence from recent works imply mechanisms of long-range Wnt signaling by cytonemes and exosomes (Gross et al., 2012; Routledge and Scholpp, 2019; Saha et al., 2016; Stanganello et al., 2015). For example, in zebrafish blastomere, Wnt8a is transported to neighboring cells through a long cytoneme projection, and successfully triggers signaling cascade activation (Stanganello et al., 2015); in mouse and human cell cultures, biologically functional Wnt3a is observed on the exosomes through immunoblot and rescue assay (Gross et al., 2012). To test if NRT-BFP-LIN-44 can function as a long range cue through those mechanisms, we examined the phenotypes of DA9 synaptic patterning and DD6 axon termination, which are known to be regulated by LIN-44 gradient (Klassen and Shen, 2007; Maro et al., 2009; Mizumoto and Shen, 2013).

DA9 is a cholinergic motor neuron whose cell body resides in the preanal ganglion, and it initially extends an axon posteriorly along the ventral nerve cord, and later joining the dorsal nerve cord through a commissure. It forms *en passant* synapses onto dorsal body wall muscles, but only within a designated region, and also creates a synapse-free (or asynaptic) domain (**Figure 10A**). The posterior asynaptic domain is regulated by LIN-44 gradient: when LIN-44 is

absent, DA9 forms ectopic synapses within that region (**Figure 10B**); when *lin-44* is overexpressed , the asynaptic domain enlarges, suggesting synapse formation is negatively regulated by a LIN-44 gradient (Klassen and Shen, 2007). Similarly, the termination of axon outgrowth in DD6 GABAergic motor neuron is also dependent on LIN-44 gradient. In wildtype animals, DD6 axon terminates before it reaches to the rectum region. In *lin-44* null mutants, it overshoots beyond the rectum region (**Figure 10E**); and in the case of *lin-44* overexpression, DD6 axon is abnormally short (Maro et al., 2009).

We examined these two phenotypes in *nrt-bfp-lin-44* animals, and found they have similar defects to *lin-44* loss of function mutants (**Figure 10C-F**). This observation suggests membrane-tethered LIN-44 does not form a gradient and reach DA9 and DD6. In DA9, LIN-17::mCherry puncta are localized at the asynaptic region in a *lin-44* dependent manner (Klassen and Shen, 2007; Mizumoto and Shen, 2013) (**Figure 10A, B**). In addition, we did not observe LIN-17::mCherry puncta in *nrt-bfp-lin-44* animals (**Figure 10C**), which is a marker for Wnt signaling activation caused by LIN-44/Wnt (Klassen and Shen, 2007). Overall, these observations suggests LIN-44 gradient is required in DA9 synapse formation and DD6 axon termination, but not in PDB neurite pruning (**Figure 10G**).

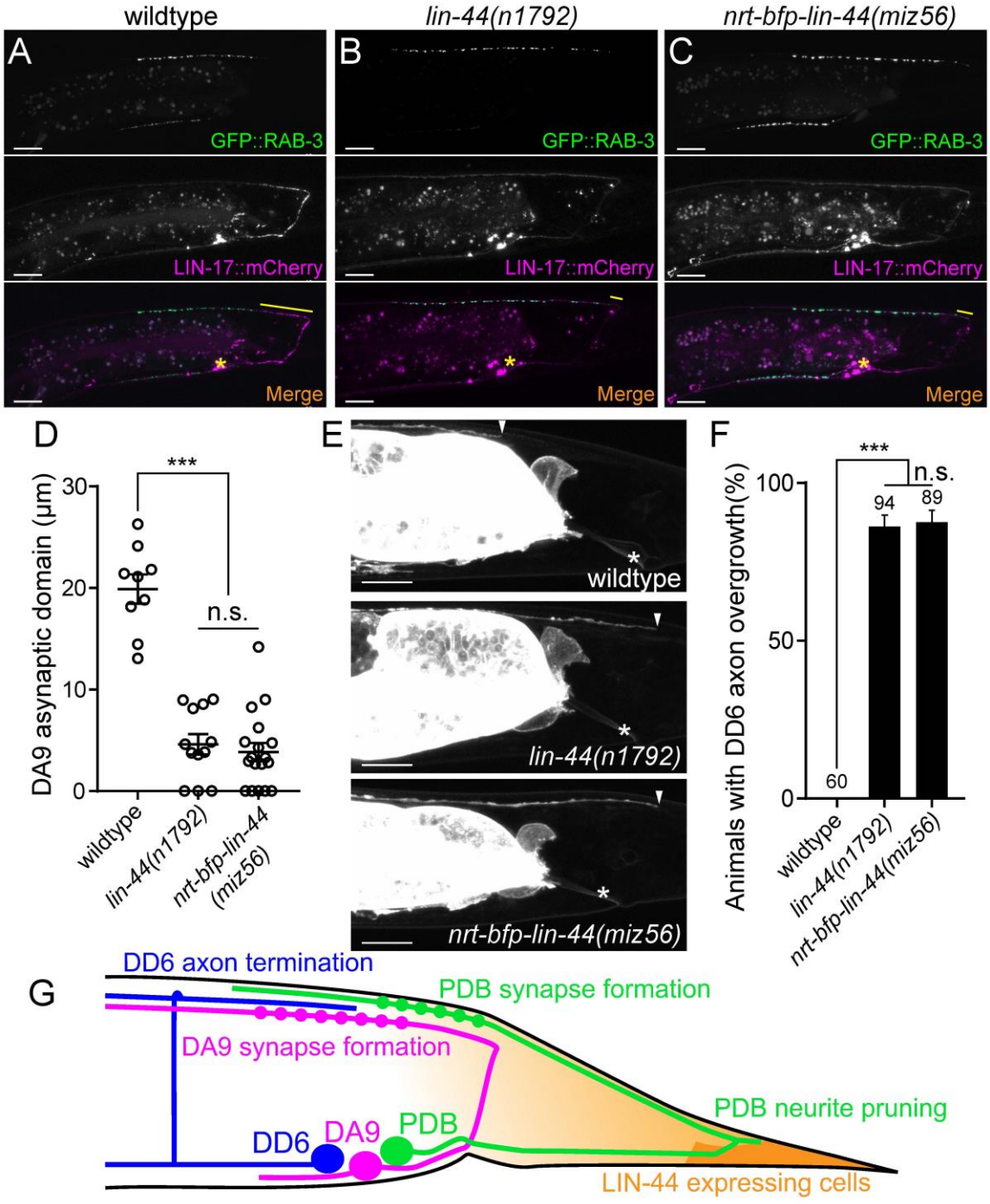
wildtype
lin-44(n1792)
nrt-bfp-lin-44(miz56)
A
B
C
GFP::RAB-3
LIN-17::mCherry
Merge
D
DA9 asynaptic domain (μm)
***
n.s.
wildtype
lin-44(n1792)
nrt-bfp-lin-44 (miz56)
E
wildtype
lin-44(n1792)
nrt-bfp-lin-44(miz56)
F
Animals with DD6 axon overgrowth(%)
***
n.s.
94
89
60
G
DD6 axon termination
PDB synapse formation
DA9 synapse formation
PDB neurite pruning
DD6
DA9
PDB
LIN-44 expressing cells

Figure 10. Membrane-tethered LIN-44 does not function as a gradient signal. (**A-C**) Representative images of DA9 presynaptic specializations labeled with GFP::RAB-3 (top panels), LIN-17::mCherry localization (middle panels) and merged images (bottom panels) in N2 (**A**), *lin-44(n1792)* (**B**) and *nrt-bfp-lin-44(miz56)* (**C**) animals. Asterisks denote DA9 cell body, and yellow lines represent the posterior asynaptic domain of the DA9 dorsal axon. GFP::RAB-3 puncta in the ventral side of the worm is due to the expression of P*mig-13::gfp::rab-3* in the VA12 motor neuron. (**D**) Quantification of the DA9 asynaptic domain length. The DA9 asynaptic domain is defined by the distance between the most posterior mCherry::RAB-3 puncta and the DA9 commissure. Each dot represents an individual animal. Error bars indicate mean ± SEM. ***p<0.001; n.s., not significant (one-way ANOVA). (**E**) Representative image of DD6 posterior axon in wildtype (top panel), *lin-44(n1792)* (middle panel) and *nrt-bfp-lin-44(miz56)* (bottom panel). Asterisks denote the position of the rectum; arrowheads denote the end of DD6 axon. (**F**) Quantification of DD6 axon overgrowth defect. Animals were considered as defective if DD6 axon terminal was located posteriorly to the rectum. *** p<0.001; n.s., not significant (Chi-square test). Error bars represent standard error of proportion (SEP). (**G**) Schematic of the relative positions of DD6, DA9, PDB neurons and *lin-44* expressing cells. Light graded orange represents hypothetical LIN-44 gradient. Scale bars: 10μm.

We further tested if NRT-BFP-LIN-44 is sufficient for replacing the function of diffusible LIN-44 in other aspects of PDB development. In *lin-44* null mutants, PDB exhibits defects in cell fate specification and neurite guidance (**Figure 5B**). These defects are likely due to the lack of LIN-44 gradient signal since the PDB cell body and target growthcone are located away from the *lin-44*-expressing cells. The penetrance of these defects in PDB of *nrt-bfp-lin-44*

was comparable to those of *lin-44* null mutants (**Figure 5B**), suggesting that PDB requires both gradient-dependent and independent LIN-44/Wnt signal for normal development. Consistent with this idea, we found that the position of presynaptic RAB-3 puncta in the PDB neuron is dependent on the LIN-44 gradient. Similar to DA9, the PDB neuron has a large asynaptic domain in the dorsal neurite (**Figure 11A**). In both *lin-44* null and *nrt-bfp-lin-44* animals, we observed ectopic mCherry::RAB-3 puncta in this neurite domain (**Figure 11A, B**). This result suggests that PDB can respond to diffusible and non-diffusible Wnt signal in a context-dependent manner: it utilizes LIN-44 gradient signal to determine its cell fate, neurite guidance and the subcellular localization of the presynaptic vesicles, while its neurite pruning is induced by gradient-independent LIN-44 signal.

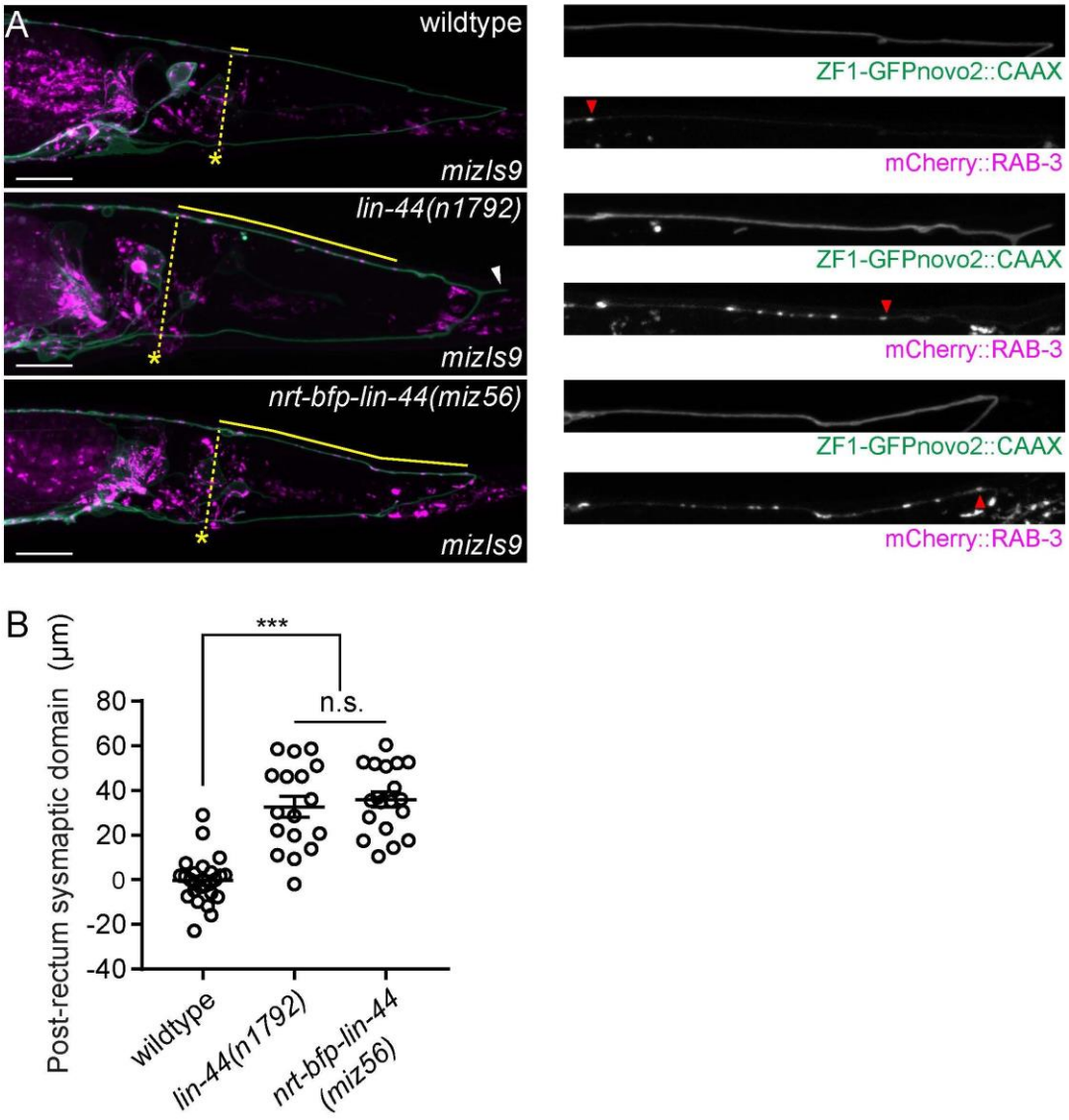

Figure 11. LIN-44 gradient-dependent localization of RAB-3 in PDB.

(A) Representative image of the PDB structure and presynaptic marker localization labeled with *mizIs9* PDB marker in wildtype (top), *lin-44* null (middle) and *nrt-bfp-lin-44* (bottom) animals. The dotted lines indicate the minimum distance from the anus to the dorsal neurite of PDB, which was used as a reference point to quantify the relative position of RAB-3 puncta in the dorsal neurite of PDB. Solid yellow lines represent the distance between the reference point and the most posterior RAB-3 puncta in each genotype. Magnified images of the dorsal neurite of

PDB in green (ZF1-GFPnovo2::CAAX) and red (mCherry::RAB-3) channels are shown in the right panels. (**B**) Quantification of the RAB-3 puncta localization. The value represents the distance from the reference point in the dorsal neurite of PDB to the most posterior RAB-3 punctum. Positive and negative values indicate that the most posterior RAB-3 punctum is located posteriorly or anteriorly to the reference point, respectively. Error bars indicate mean ± SEM. ***p<0.001; n.s., not significant (one-way ANOVA).

3.4 Wnt signaling pathway is asymmetrically activated

3.4.1 LIN-17/Fz localizes asymmetrically in the posterior neurites of PDB

A hallmark of activated Wnt signaling pathway is subcellular localization of Frizzled proteins (Goldstein et al., 2006; Hilliard and Bargmann, 2006; Wu and Herman, 2007). To visualize the localization of LIN-17/Fz in the PDB neurites, we expressed the functional LIN-17::GFP fusion protein along with the cytoplasmic BFP in the PDB neuron. In wild-type background, the pruning posterior neurite tended to have bright LIN-17::GFP puncta, while the non-pruning anterior neurite did not have any visible punctum (**Figure 12A**). This trend was quantitatively confirmed by comparing GFP/BFP signal intensity ratio in the anterior growth cone versus posterior dorsal neurite growthcone (**Figure 12D**).

3.4.2 LIN-17/Fz asymmetrical localization is dependent on LIN-44/Wnt

Based on our model, the high LIN-17/Fz localization on the posterior neurites is derived by exposure to the high LIN-44/Wnt, which is distributed around the LIN-44 expressing cells around the tail tip. Consistently, we found this asymmetric localization of LIN-17::GFP is disrupted in *lin-44(n1792)* mutants. In those animals, posterior neurites do not have LIN-

17::GFP puncta (**Figure 12B, D**). We also examined LIN-17::GFP distribution pattern in *nrt-bfp-lin-44(miz56)*, and found that the asymmetric LIN-17::GFP localization is restored, suggesting NRT-BFP-LIN-44 can be recognized by LIN-17 (**Figure 12C, D**).

It is to be noted that the LIN-17 puncta observed on the ventral neurite between cell body and primary branch in N2 animals are absent in *lin-44(n1792)* and *lin-44(miz56)* animals. This may be caused by the long-range LIN-44 gradient, which is abolished in both *lin-44* mutants.

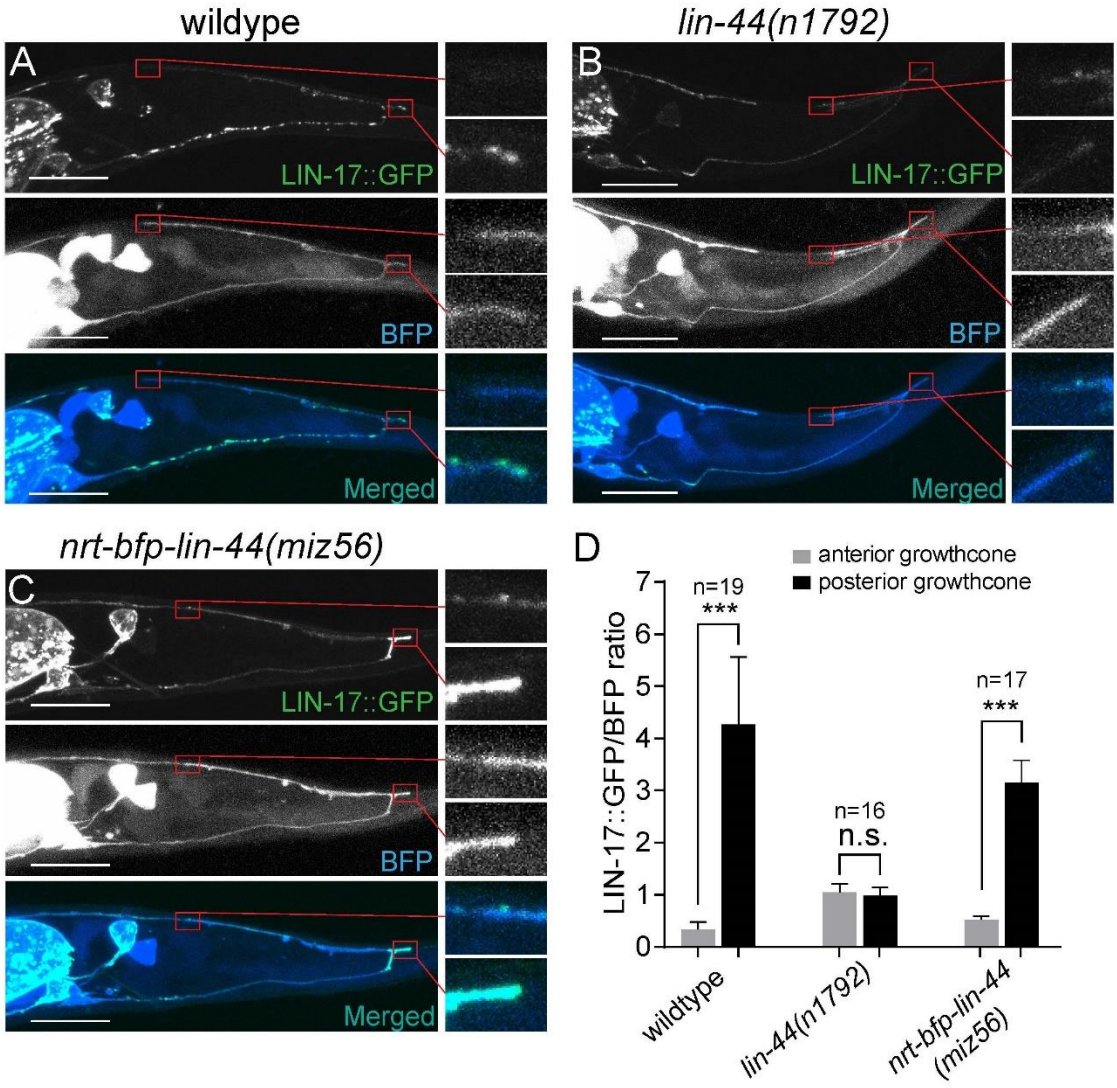

Figure 12. LIN-44/Wnt-dependent localization of LIN-17/Fz at the PDB posterior neurites. (**A-C**) Representative images of LIN-17::GFP localization (top panels), PDB neurite structure labeled with cytoplasmic BFP (middle panels) and merged images (bottom panels) in wildtype (**A**), *lin-44(n1792)* (**B**), and *nrt-bfp-lin-44(miz56)* (**C**) animals, respectively. Magnified images of the tip of anterior and posterior neurites are shown in the right panels. (**D**) Quantification of the normalized GFP/BFP signal ratio at the anterior and posterior growth cones. Error bars indicate mean ± SEM. ***p<0.001; n.s., not significant (Ratio paired t-test).

3.4.3 Wnt signaling recruits Dishevelled to the PDB posterior neurites

We then tested the localization of Dishevelled, the downstream protein of LIN-17/Fz. In *C. elegans, dsh-1* has been reported to function downstream of *lin-17*/Frizzled, and consequently has asymmetrical subcellular localization (Klassen and Shen, 2007; Mizumoto and Sawa, 2007). To visualize the localization of DSH-1 in PDB, we expressed DSH-1::GFPnovo2 together with the cytoplasmic BFP (Axelrod, 2001).

Similar to LIN-17, in N2 and *lin-44(miz56)* animals, DSH-1 is asymmetrically localized at the posterior neurites, while in *lin-44(n1792)* animals, the asymmetric localization of DSH-1 disappeared (**Figure 13A, B, D, E**). Consistent with our hypothesis that LIN-17 is the sole receptor for LIN-44 in neurite pruning, DSH-1 is not enriched in the posterior neurites in *lin-17(n671)* animals, similar to *lin-44(n1792)* (**Figure 13C, E**). We did not observe any defect in PDB neurite structure in loss of function *dsh-1* mutants (**Figure 5B**), possibly due to the functional redundancy among the Dishevelled genes. In *C. elegans*. There are 3 genes encoding for Dishevelled proteins (*mig-5, dsh-1* and *dsh-2*). In this study, we focused on *mig-5* and *dsh-1*, because they have been reported to have functions post-embryonically. Similar to *dsh-1* mutants, *mig-5* mutants are also superficially wildtype. To check if these two genes function redundantly,

we also checked *mig-5;dsh-1* double mutants. Those animals are barely viable, and brief microscopy observation suggests they may have severe linage defects, which prohibits us from further exploration.

Taken together, we propose that LIN-44/Wnt forms a local distribution pattern around the *lin-44*-expressing hypodermal cells. Upon physical contact between PDB neurites and the *lin-44*expressing cells, Wnt signaling cascade is activated through LIN-17/Fz, and thereby recruits downstream protein DSH-1, in the posterior neurites but not the anterior neurite. When LIN-44 is absent, LIN-17/Fz and Dishevelled proteins are not activated, thus the pruning of posterior neurite is defective (**Figure 14**).

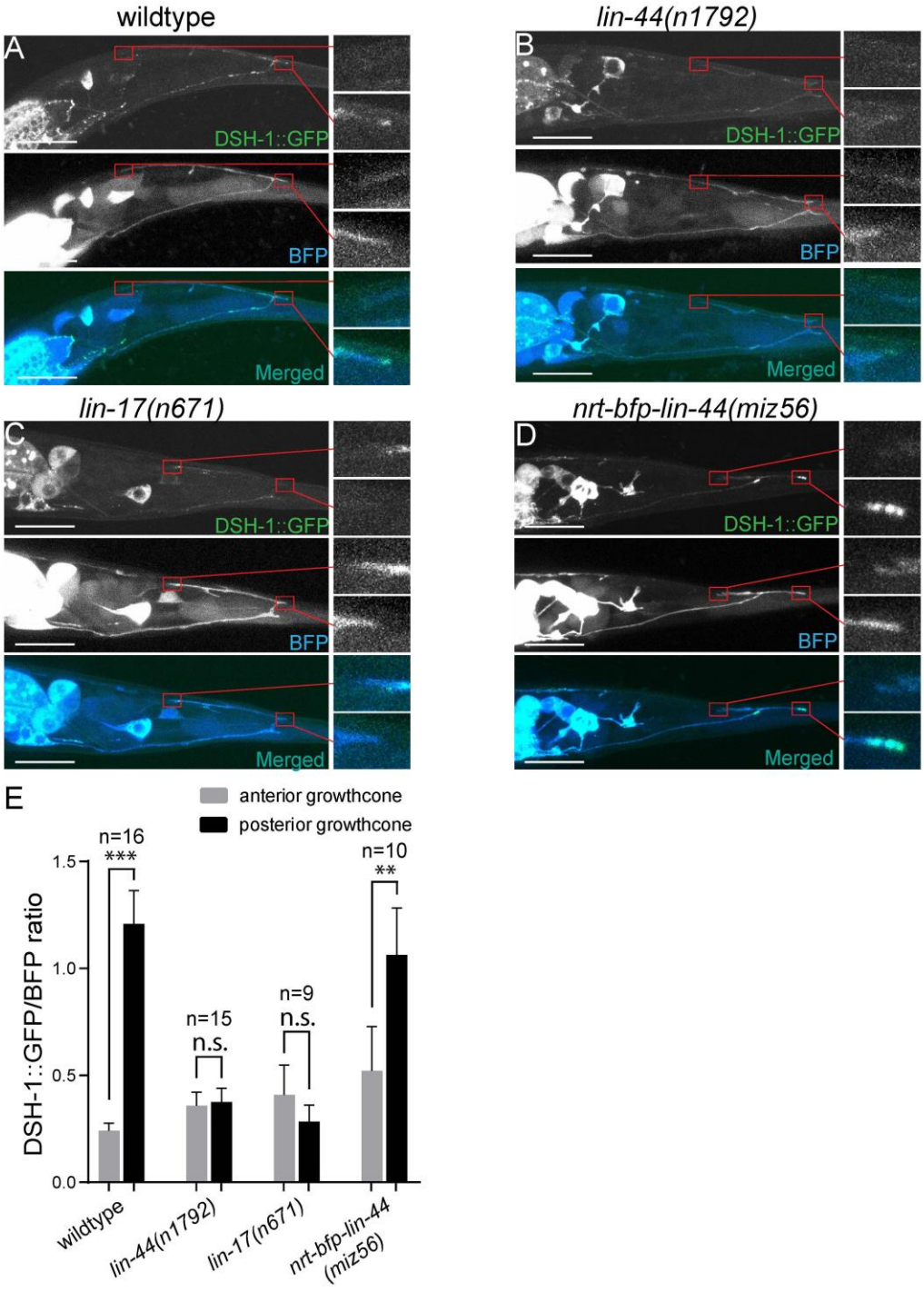
wildtype
A
DSH-1::GFP
BFP
Merged
lin-44(n1792)
B
DSH-1::GFP
BFP
Merged
lin-17(n671)
C
DSH-1::GFP
BFP
Merged
nrt-bfp-lin-44(miz56)
D
DSH-1::GFP
BFP
Merged
E
anterior growthcone
posterior growthcone
DSH-1::GFP/BFP ratio
1.5
1.0
0.5
0.0
n=16
***
n=15
n.s.
n=9
n.s.
n=10
**
wildtype
lin-44(n1792)
lin-17(n671)
nrt-bfp-lin-44 (miz56)

Figure 13. Wnt-dependent localization of DSH-1/Dsh at the PDB posterior neurites. (**A-D**) Representative images of DSH-1::GFP localization (top panels), PDB neurite structure labeled with cytoplasmic BFP (middle panels) and merged images (bottom panels) in wildtype (**A**), *lin-44(n1792)* (**B**), *lin-17(n671)* (**C**) and *nrt-bfp-lin-44(miz56)* (**D**) animals, respectively. Magnified images of the tip of anterior and posterior neurites are shown in the right panels. (**E**) Quantification of the normalized GFP/BFP signal ratio at the anterior and posterior growth cones. Error bars indicate mean ± SEM. ***p<0.001; n.s., not significant (Ratio paired t-test).

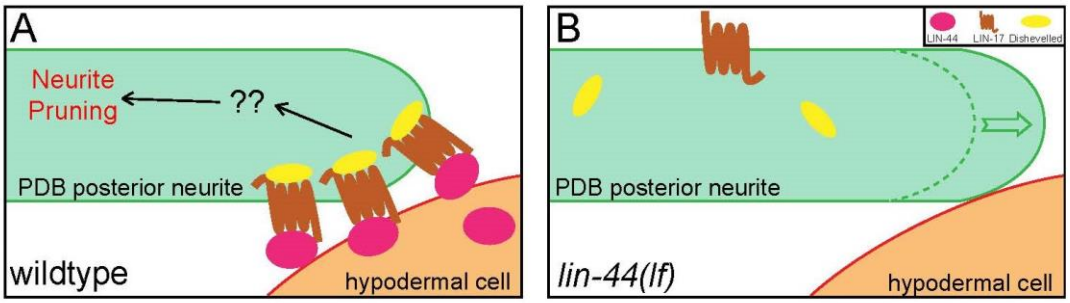

Figure 14. A model of neurite pruning in PDB. Local and high concentration of LIN-44/Wnt from the tail hypodermal cell (hyp10) induces PDB neurite pruning via recruiting LIN-17/Fz and DSH-1/Dsh in wildtype (left panel) and defective pruning in *lin-44* mutants (right panel).

3.5 Calcium, Wnt-calcium pathway and neurite pruning

There are 3 signaling cascades of Wnt signaling. Depending on the receptor context, the same ligand may activate different Wnt signaling cascades (Bejsovec, 2005; Kikuchi et al., 2011). To investigate through which pathway LIN-44 and LIN-17 mediates PDB neurite pruning, we tested several key genes in the canonical Wnt and planar cell polarity (PCP) pathway. We found mutants with knocked out *bar-1*, a β-catenin homolog in *C. elegans*, had a high penetrance phenotype of missing PDB, but animals with successfully generated PDB neurite do not have visible structural defect (**Figure 5B**). This is consistent with our observation that *lin-44* and *lin-17* mutants tend to have missing PDB, and also consistent with an early report of Wnts function in the division of PDB precursor cells (Jiang and Sternberg, 1998). Taken together, we believe that through the β-catenin pathway, LIN-44 and LIN-17 regulate PDB cell linage, but not neurite pruning.

Several key genes in PCP pathway were also tested in this study: *fmi-1/flamingo*, *vang-1/Van Gogh and cam-1/ROR*, which have been reported to play important roles in Wnt PCP signaling, and mediate neuronal development in different aspects (Chien et al., 2015; Hayashi et al., 2009; Klassen and Shen, 2007). However, mutants of those genes showed no defect in neurite pruning (**Figure 5B**), suggesting the PCP pathway is not involved in the pruning process of PDB posterior neurites.

Frizzled protein, the putative Wnt receptor, has been reported to cause a calcium surge through the Wnt-calcium pathway (Katanaev et al., 2005; Kohn and Moon, 2005; D. C. Slusarski et al., 1997). Furthermore, a calcium transient is observed prior to *Drosophila* dendritic pruning,

dependent on VGCCs, and thereby activates calpain proteases to induce pruning in designated dendrites (Kanamori et al., 2013). In *C. elegans,* despite there are homologs of a few key genes exists (*egl-8*/PLC, *itr-1*/IP_3R, *plc-1*/phospholipase C), and some evidences suggests those genes are required in behavior and cell migration (Thomas-Virnig et al., 2004; Vázquez-Manrique et al., 2008; Walker et al., 2009), Wnt-Calcium pathway has not been directly reported. By the method of exclusion, the current data from this study infers that Wnt-calcium pathway may regulates PDB neurite pruning. Unfortunately, several attempts using a GCamP reporter and expressing a calbindin construct as a calcium chelator (Schumacher et al., 2012) have failed to visualize or manipulate calcium mobilization in PDB during pruning, possibly due to the late onset of the *kal-1* promoter. We also attempted to examine genes encoding for VGCCs and calpain in *C. elegans*, and looked for defects at the L4 stage, but none of the 6 VGCC subunit genes we have tested (*unc-2, nca-2*, *egl-19*, *egl-19*, *unc-77, unc-36*), and 2 calpains (*clp-1, clp-3*) showed any visible defect. These observations do not completely disapprove our hypothesis that Wnt instruct neurite pruning through calcium pathway, since VGCC is not the sole source for cytoplasmic calcium, and there are 3 other calpain genes (*clp-4, clp-6, clp-7*) in *C. elegans* that were not tested in this study.

3.6 E3 ligase EEL-1/HUWE1 is required in PDB neurite pruning

While examining CB251, a strain containing an *unc-36(e251)* allele, we accidentally found a spontaneous mutation that causes PDB neurite pruning defect. Whole genome sequencing revealed a point mutation in *eel-1* that creates an E to K mutation, close to the HECT domain. The gene *eel-1* contains a conserved HECT domain, subclass of E3 ubiquitin protein ligase, orthologous to human HUWE1. A study suggests EEL-1 functions as an inhibitor of Wnt signaling in Q cell migration in *C. elegans*. In mouse cells, Huwe1 promotes ubiquitylation of

Dvl protein, and possibly down regulates Wnts signaling by inhibiting the multimerization of Dvl (de Groot et al., 2014). However, our observation can not be explained by *eel-1* down regulating Wnt, and in *eel-1(ok1575)* loss of function mutant, we also did not observe any defect in DSH-1::GFP aggregation (**Figure 15A, B**), suggesting *eel-1* does not affect the asymmetrical activation of Wnt in PDB neurite pruning.

During neurite pruning, the removal of the existent neurite structure requires proper protein degradation. In *Drosophila*, the ubiquitin-proteasome system (UPS) is reported to play important roles in MB γ neuron axon pruning (Watts et al., 2003) and C4da neuron dendrite pruning (Kuo et al., 2005). Expression of yeast ubiquitin protease, an antagonist of ubiquitin ligase, in those neurons is sufficient to induce pruning defects. These findings bring a possible explanation that *eel-1* may be controlled by *lin-44/Wnt* pathway, and assists ubiquitylation of other proteins, but not functions as a negative regulator of Wnt to disrupt the direct downstream protein DSH-1. A few attempts on generating *lin-44;eel-1* double mutant has been failed, therefore we were not able to have a clear conclusion to this question.

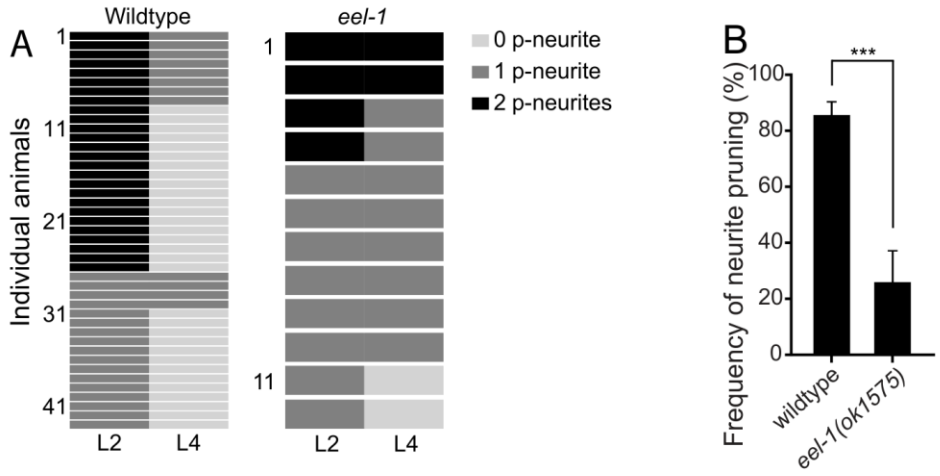

Figure 15. *eel-1* is required for the posterior neurite pruning.

(**A**) Quantification of the posterior neurite number of individual animals at L2 and L4 stages in wildtype and *eel-1(ok1575).* (**B**) Quantification of the posterior neurite pruning frequency. *** p < 0.001; n.s., not significant (Chi-square with Yates' correction). Error bars represent standard error of proportion (SEP).

3.7 Screening of other signaling pathways and genes

Other than the components of Wnt signaling pathway, during the initial reverse genetic screening, we also examined a few other genes that have been reported to function in axon guidance, such as netrin (*unc-6, unc-5*) (Chan et al., 1996), slit-robo (*sax-3*) (Fujisawa, 2007), neuron navigator-1 (*unc-53*) (Maes et al., 2002), and *unc-129/TGFβ* (Colavita et al., 1998), but mutants in none of these genes showed noticeable pruning defects. Noteworthy, *unc-6* and *unc-5* mutants showed dorsal-ventral guidance defect, which is consistent to their reported function in other neurons such as VDs (Norris and Lundquist, 2011); *unc-129* mutants showed guidance defect of the anterior neurite, suggesting the growth cone pathfinding of PDB after the pruning event still requires aids from other signaling pathways.

4. Discussion

Dynamic neurite arbor formation during neuron development is commonly seen under different contexts (Niell et al., 2004; Wu et al., 1999), however, how does a neuron select neurites for pruning is one of the most interesting questions. In the case of stereotypical neurite pruning, certain neurites are always pruned from animal to animals, suggesting the existence of external guidance cues in the environment. In this study we discovered a novel function of Wnt

in instructing neurite pruning in *C. elegans*, where *lin-44/Wnt* instructs the removal of posterior neurites in PDB, through the direct contact with its expressing cells. Furthermore, our result also suggests the molecule LIN-44 functions not only at short-range but also at long-range in *C. elegans*, and membrane-tethered modification can precisely abolish the long-range function, while leaving the short-range function unaffected.

4.1 Wnt instructs neurite pruning independent of neuronal activity

Neurite pruning is an important process in the development of the nervous system. The molecular mechanisms by which certain neurites are stabilized while others are pruned are still not thoroughly studied. Based on its relationship with neuronal activity, neurite pruning can be classified as activity-dependent and activity-independent.

In order to explain the mechanism of learning, over half century ago, Donald Hebb hypothesized that the connections among neurons follow the rule "use it or lose it": only the constantly activated connections are preserved during development, while the others are not (Hebb, 1949; Miller et al., 2000). In the case of activity-dependent neurite pruning, the sculpting of circuits is regulated by neuronal input and synapse formation, similar to Hebbian theory, which will eventually contribute to learning and memory formation (Cline, 2003). On the other hand, activity-independent neurite pruning requires specific molecular markers existing in the extracellular matrix, therefore the map of the connectome is pre-determined by the expression of a series of genes (Meyer, 1998). In this study, we used *unc-13(lf)* to mimic the loss of neuronal activity, and found no defect in the pruning of PDB, suggesting the process is likely activity independent.

One of the best established morphogens, Wnt, is reported to have important functions in neural development, providing guidance for cell migration, polarity, neurite guidance and synapse formation, and therefore has the potency to serve as a molecular marker to instruct neurite pruning. However, the function of Wnt in neurite pruning is scantly reported from two studies, and the results are inconclusive (Hayashi et al., 2009; A. P. Singh et al., 2010).

In the post-larval pruning of *Drosophila* CSDns dendrite, Wnt is reported to instruct dendritic pruning, and antagonized by glutamatergic synaptic input. During the development of CSDn, its dendrites arbor extensively, and similar to our observation, the excessive dendritic arbors are pruned under the instruction of Wnts. However, the mechanism of preserving "correct" dendrite in CSDns is dependent on NMDAR, which is recruited by synaptic input from other neurons and antagonize the pruning from Wnt (A. P. Singh et al., 2010), while in PDB, the Wnt signaling inducing neurite pruning is spatially restrained, and does not require synaptic activity.

In the pruning of *C. elegans* AIM neuron, two other worm Wnts CWN-1 and CWN-2 serve as trophic cues through their receptor CAM-1, and protect AIM neurite against the pruning initiated by UNC-86-MBR-1 signaling cascade (Hayashi et al., 2009; Kage et al., 2005). Knocking out *cam-1* can rescue the pruning defect in *mbr-1* mutants, and *cam-1* overexpression can inhibit normal neurite pruning in wildtype animals (Hayashi et al., 2009). The controversy between their observation and ours can be explained by the difference in Wnts and receptors, and except for the two above-mentioned transcription factors UNC-86 and MBR-1, the instructive cues in AIM neurite pruning also remains unclear.

Our study provides additional evidence for Wnt instructs neurite pruning, which functions in an activity independent manner, and the pruning activity is restrained by the relative position of the neurites and Wnt producing cells.

4.2 Co-existence of gradient-independent and gradient dependent Wnt signaling

Wnt signaling is essential in many different contexts, and the target cells are often at a long range from the Wnt producing cells. Antibody also revealed that Wg staining signal is high at close range, and spreads from the source cells (Zecca et al., 1996), suggesting it has the ability to form a gradient. However, membrane-tethered Wingless *(nrt-wg)* abolishes its ability to form a visible gradient (Zecca et al., 1996), but still functions normally in *drosophila* wingdisc development, suggesting Wnt may function in a gradient-independent manner (Alexandre et al., 2014). On the other hand, they also noticed the larvae development speed and fitness is slightly affected in *NRT-Wg* animals, suggesting the Wg gradient is required elsewhere (Alexandre et al., 2014). Similarly, recent works revealed the critical requirement of secretion and diffusion of Wingless for renal tube patterning and intestinal compartmentalization in *Drosophila* (Beaven and Denholm, 2018; Tian et al., 2019).

In this study, we proposed a gradient independent function of LIN-44/Wnt in regulating neurite pruning in PDB, and testified this idea through membrane-tethered worm Wnt *(nrt-bfp-lin-44)*. In addition, we reported membrane-tethered Wnt only functioned in the pruning of PDB, but did not function as wild-type Wnt in other Wnt-related events, such as DA synaptic patterning and DD axon outgrowth (Klassen and Shen, 2007; Maro et al., 2009; Mizumoto and Shen, 2013). More interestingly, we also noticed that the level of guidance defect and linage defect of PDB is comparable between *lin-44(lf)* and *nrt-lin-44*, and reported the synaptic defect level in PDB is also not significantly changed.

The mechanisms that PDB adopt to distinguish between gradient and membrane tethered Wnt is fairly interesting. There are two hypothesises that can explain why membrane tethered Wnt and normal Wnt behave differently: concentration threshold and intracellular transportation. The first model hypothesized a threshold difference between neurite pruning and other biological processes, both membrane-tethered Wnt normal Wnt create a highly concentrated layer of Wnt around the secreting cells due to the neurotactin residue or the hydrophobicity from the palmitoyl modification, which exceeds the threshold for neurite pruning. However the attached neurotactin completely prevent the molecule from long range distribution, while a small proportion of the wild-type Wnt is able to travel for 10-50μm and reach the lower threshold for PDB differentiate, axon guidance and synaptic formation. The second hypothesis is that a proportion of Wnt can be transported on or within PDB after its binding with LIN-17/Fz. The activation of Wnt requires binding and internalization of the Wnt-Fz complex (Brunt and Scholpp, 2018), during this process, the complex may have the potential to travel for a certain distance, and thereby activates the pathway away from the Wnt producing cells.

Our result not only confirmed that the requirement of Wnt gradient is context-dependent (Alexandre et al., 2014; Beaven and Denholm, 2018; Tian et al., 2019), it also suggests a coexistence of gradient-dependent and gradient-independent function of LIN-44/Wnt in a single cell for the first time.

4.3 Asymmetrical neurite pruning of PDB

When we look at the pruning process in close range, one of the interesting things we have found is that anterior neurite can “escape” from the pruning force, even though the growth cone is only micrometers away from LIN-44 producing cells. Immunostaining data showed the intensity of Wg is much higher around the expressing cells comparing to the surrounding

environment (Alexandre et al., 2014; Zecca et al., 1996), and our observation of downstream LIN-17::GFP and DSH-1::GFP aggregation also suggests that during the pruning process, both wildtype and *nrt-lin-44* animals can recruit those downstream proteins selectively at the posterior neurites. There are a few models that can explain this observation: one is that the activation of neurite pruning requires a distinct threshold of Wnt concentration, which can be provided by both wildtype Wnt and also membrane-tethered Wnt. The other model is that unknown molecules serve as transmembrane co-factors to induce pruning from the hypodermal cells, therefore the pruning activity is only restrained at the posterior neurite. *sdn-1/syndecan* is one such candidate as it has been shown that *sdn-1* is required for the Wnt-dependent spindle orientation in early embryonic development (Dejima et al., 2014), and *sdn-1* mutants exhibit PDB structure defects similar to *lin-44/wnt* (Saied-Santiago et al., 2017). However, we did not observe significant pruning defects in PDB of *sdn-1* mutants. Further candidate and forward genetic screenings will reveal novel factors that are specifically required for the gradient-independent Wnt signaling.

4.4 Intricate development of PDB neurite

Based on our observations, we hypothesize that development of the PDB neurite involves four main processes: posterior extension of the primary branch along the ventral side, dynamic branch formation, removal of excessive branches, and anterior extension of the tertiary branch along the dorsal side. Within these processes, other than neurite pruning, two other questions still remain unresolved: How does the PDB neurite accomplish its pathfinding on the anterior-posterior and dorsal-ventral axis? What genes instruct and restrict the branch formation within the posterior region, but not anywhere else?

In the early reverse genetic screening, we observed severe guidance defect of PDB at L4 stage in the mutants of *unc-6/netrin* and its receptor *unc-5*, where the ventral and dorsal neurites are extremely short, indicating netrin signaling plays a role in the axon guidance in PDB, consistent with the previously studied function of netrin in dorsal-ventral pathfinding (Levy-Strumpf and Culotti, 2014; Norris and Lundquist, 2011). Wnt mutants, such as *lin-44, lin-17, and fmi-1* also have axon guidance defect with moderate to low penetrance, but the phenotypes are different from netrin mutants, and hard to interpret due to their complexity and low penetrance. This observation suggests a function of Wnt together with netrin in PDB axon guidance, but their relationship and mechanisms still remain unclear.

During the time-lapse imaging, we observed dynamic branch formation during the L2-L3 stage as the posterior branches start getting pruned. During this period, potential branches are frequently initiated from primary or tertiary branches, and those dynamic branches are constantly getting removed in wildtype animals. Similar behavior has also been observed in the dendritic branch formation of PVD neuron, where candidate branches tend to form dynamically within a distinct time window, and only some of them will be stabilized (Smith et al., 2010). In PVD dendrites, the formation of dendrite is initiated and stabilized by cell adhesion molecule SAX-7 from the hypodermal side (Dong et al., 2013). However, *sax-7(nj48)* mutants do not have any phenotype in PDB, suggesting this protein does not play the main role in the development of PDB. Taken together, other than the pruning process we have discussed in this study, there are many other interesting questions we can explore using PDB as a model system.

5. Bibliography

Adler PN. 2002. Planar Signaling and Morphogenesis in Drosophila. *Developmental Cell* **2**:525–535. doi:https://doi.org/10.1016/S1534-5807(02)00176-4

Alexandre C, Baena-Lopez A, Vincent JP. 2014. Patterning and growth control by membrane-tethered wingless. *Nature* **505**:180–185. doi:10.1038/nature12879

Armenti ST, Lohmer LL, Sherwood DR, Nance J. 2014. Repurposing an endogenous degradation system for rapid and targeted depletion of C. elegans proteins. *Development* **141**:4640–4647. doi:10.1242/dev.115048

Arnés M, Casas Tintó S. 2017. Aberrant Wnt signaling: a special focus in CNS diseases. *Journal of Neurogenetics* **31**:216–222. doi:10.1080/01677063.2017.1338696

Au V, Li-Leger E, Raymant G, Flibotte S, Chen G, Martin K, Fernando L, Doell C, Rosell FI, Wang S, Edgley ML, Rougvie AE, Hutter H, Moerman DG. 2019. CRISPR/Cas9 Methodology for the Generation of Knockout Deletions in Caenorhabditis elegans. *G3: Genes|Genomes|Genetics* **9**:135–144. doi:10.1534/g3.118.200778

Axelrod JD. 2001. Unipolar membrane association of Dishevelled mediates Frizzled planar cell polarity signaling. *Genes and Development* **15**:1182–1187. doi:10.1101/gad.890501

Babu P. 1977. Early developmental subdivisions of the wing disk in Drosophila. *Molecular & general genetics : MGG* **151**:289–94.

Bagri A, Cheng HJ, Yaron A, Pleasure SJ, Tessier-Lavigne M. 2003. Stereotyped pruning of long hippocampal axon branches triggered by retraction inducers of the semaphorin family. *Cell* **113**:285–299. doi:10.1016/S0092-8674(03)00267-8

Bänziger C, Soldini D, Schütt C, Zipperlen P, Hausmann G, Basler K. 2006. Wntless, a Conserved Membrane Protein Dedicated to the Secretion of Wnt Proteins from Signaling Cells. *Cell* **125**:509–522. doi:10.1016/j.cell.2006.02.049

Beaven R, Denholm B. 2018. Release and spread of Wingless is required to pattern the proximo-distal axis of Drosophila renal tubules. *eLife* **7**:1–17. doi:10.7554/eLife.35373

Bejsovec A. 2005. Wnt pathway activation: New relations and locations. *Cell* **120**:11–14. doi:10.1016/j.cell.2004.12.021

Bindels DS, Haarbosch L, Van Weeren L, Postma M, Wiese KE, Mastop M, Aumonier S, Gotthard G, Royant A, Hink MA, Gadella TWJ. 2016. MScarlet: A bright monomeric red fluorescent protein for cellular imaging. *Nature Methods* **14**:53–56. doi:10.1038/nmeth.4074

Brenner S. 1974. The genetics of Caenorhabditis elegans. *Genetics* **77**:71–94. doi:10.1002/cbic.200300625

Brunt L, Scholpp S. 2018. The function of endocytosis in Wnt signaling. *Cellular and Molecular Life Sciences* **75**:785–795. doi:10.1007/s00018-017-2654-2

Buechler J, Salinas PC. 2018. Deficient Wnt Signaling and Synaptic Vulnerability in Alzheimer's Disease: Emerging Roles for the LRP6 Receptor. *Frontiers in Synaptic Neuroscience* **10**:1–10. doi:10.3389/fnsyn.2018.00038

Bülow HE, Berry KL, Topper LH, Peles E, Hobert O. 2002. Heparan sulfate proteoglycan-dependent induction of axon branching and axon misrouting by the Kallmann syndrome

gene kal-1. *Proceedings of the National Academy of Sciences* **99**:6346–6351. doi:10.1073/pnas.092128099

Cadigan KM, Fish MP, Rulifson EJ, Nusse R. 1998. Wingless repression of Drosophila frizzled 2 expression SHAPES THE wingless morphogen gradient in the wing. *Cell* **93**:767–777. doi:10.1016/S0092-8674(00)81438-5

Cang J, Wang L, Stryker MP, Feldheim DA. 2008. Roles of Ephrin-As and Structured Activity in the Development of Functional Maps in the Superior Colliculus. *Journal of Neuroscience* **28**:11015–11023. doi:10.1523/JNEUROSCI.2478-08.2008

Caricasole A. 2004. Induction of Dickkopf-1, a Negative Modulator of the Wnt Pathway, Is Associated with Neuronal Degeneration in Alzheimer's Brain. *Journal of Neuroscience* **24**:6021–6027. doi:10.1523/jneurosci.1381-04.2004

Chan SS-Y, Zheng H, Su M-W, Wilk R, Killeen MT, Hedgecock EM, Culotti JG. 1996. UNC-40, a C. elegans Homolog of DCC (Deleted in Colorectal Cancer), Is Required in Motile Cells Responding to UNC-6 Netrin Cues. *Cell* **87**:187–195. doi:10.1016/S0092-8674(00)81337-9

Chen H, Bagri A, Zupicich JA, Zou Y, Stoeckli E, Pleasure SJ, Lowenstein DH, Skarnes WC, Chédotal A, Tessier-Lavigne M. 2000. Neuropilin-2 Regulates the Development of Select Cranial and Sensory Nerves and Hippocampal Mossy Fiber Projections. *Neuron* **25**:43–56. doi:10.1016/S0896-6273(00)80870-3

Chien SJ, Gurling M, Kim C, Craft T, Forrester W, Garriga G. 2015. Autonomous and nonautonomous regulation of Wnt-mediated neuronal polarity by the C. elegans Ror kinase CAM-1. *Developmental Biology* **404**:55–65. doi:10.1016/j.ydbio.2015.04.015

Cline H. 2003. Sperry and Hebb: oil and vinegar? *Trends in Neurosciences* **26**:655–661. doi:10.1016/j.tins.2003.10.005

Colavita A, Krishna S, Zheng H, Padgett RW, Culotti JG. 1998. Pioneer Axon Guidance by UNC-129, a C. elegans TGF-β. *Science* **281**:706–709. doi:10.1126/science.281.5377.706

Coudreuse DYM. 2006. Wnt Gradient Formation Requires Retromer Function in Wnt-Producing Cells. *Science* **312**:921–924. doi:10.1126/science.1124856

Davis EK, Zou Y, Ghosh A. 2008. Wnts acting through canonical and noncanonical signaling pathways exert opposite effects on hippocampal synapse formation. *Neural Development* **3**:1–17. doi:10.1186/1749-8104-3-32

de Groot REA, Ganji RS, Bernatik O, Lloyd-Lewis B, Seipel K, Edova K, Zdrahal Z, Dhople VM, Dale TC, Korswagen HC, Bryja V. 2014. Huwe1-Mediated Ubiquitylation of Dishevelled Defines a Negative Feedback Loop in the Wnt Signaling Pathway. *Science Signaling* **7**:ra26–ra26. doi:10.1126/scisignal.2004985

Dejima K, Kang S, Mitani S, Cosman PC, Chisholm AD. 2014. Syndecan defines precise spindle orientation by modulating Wnt signaling in C. elegans. *Journal of Cell Science* **127**:e1–e1. doi:10.1242/jcs.165761

Dong X, Liu OW, Howell AS, Shen K. 2013. An Extracellular Adhesion Molecule Complex Patterns Dendritic Branching and Morphogenesis. *Cell* **155**:296–307. doi:10.1016/j.cell.2013.08.059

Fire A. 1986. Integrative transformation of Caenorhabditis elegans. *The EMBO journal* **5**:2673–80. doi:10.1002/J.1460-2075.1986.TB04550.X

Folke J, Pakkenberg B, Brudek T. 2018. Impaired Wnt Signaling in the Prefrontal Cortex of Alzheimer's Disease. *Molecular Neurobiology* 1–19. doi:10.1007/s12035-018-1103-z

Friedland AE, Tzur YB, Esvelt KM, Colaiácovo MP, Church GM, Calarco JA. 2013. Heritable genome editing in C. elegans via a CRISPR-Cas9 system. *Nature methods* **10**:741–3. doi:10.1038/nmeth.2532

Fujisawa K. 2007. Erratum: The Slit receptor EVA-1 coactivates a SAX-3/Robo-mediated guidance signal in C. elegans (Science (1934)). *Science* **318**:570. doi:10.1126/science.318.5850.570

Gibson DG, Young L, Chuang R-Y, Venter JC, Hutchison CA, Smith HO. 2009. Enzymatic assembly of DNA molecules up to several hundred kilobases. *Nature Methods* **6**:343–345. doi:10.1038/nmeth.1318

Gleason JE, Szyleyko EA, Eisenmann DM. 2006. Multiple redundant Wnt signaling components function in two processes during C. elegans vulval development. *Developmental Biology* **298**:442–457. doi:10.1016/j.ydbio.2006.06.050

Goldstein B, Takeshita H, Mizumoto K, Sawa H. 2006. Wnt signals can function as positional cues in establishing cell polarity. *Developmental Cell* **10**:391–396. doi:10.1016/j.devcel.2005.12.016

González-Scarano F, Baltuch G. 2002. Microglia As Mediators of Inflammatory and Degenerative Diseases. *Annual Review of Neuroscience* **22**:219–240. doi:10.1146/annurev.neuro.22.1.219

Gross JC, Chaudhary V, Bartscherer K, Boutros M. 2012. Active Wnt proteins are secreted on exosomes. *Nature Cell Biology* **14**:1036–1045. doi:10.1038/ncb2574

Grueber WB, Ye B, Moore AW, Jan LY, Jan YN. 2003. Dendrites of distinct classes of Drosophila sensory neurons show different capacities for homotypic repulsion. *Current Biology* **13**:618–626. doi:10.1016/S0960-9822(03)00207-0

Hall AC, Lucas FR, Salinas PC. 2000. Axonal remodeling and synaptic differentiation in the cerebellum is regulated by WNT-7a signaling. *Cell* **100**:525–535. doi:10.1016/S0092-8674(00)80689-3

Harterink M, Kim DH, Middelkoop TC, Doan TD, van Oudenaarden A, Korswagen HC. 2011. Neuroblast migration along the anteroposterior axis of C. elegans is controlled by opposing gradients of Wnts and a secreted Frizzled-related protein. *Development* **138**:2915–2924. doi:10.1242/dev.064733

Hayashi Y, Hirotsu T, Iwata R, Kage-Nakadai E, Kunitomo H, Ishihara T, Iino Y, Kubo T. 2009. A trophic role for Wnt-Ror kinase signaling during developmental pruning in Caenorhabditis elegans. *Nature Neuroscience* **12**:981–7. doi:10.1038/nn.2347

He C, Liao C, Pan C. 2018. Wnt signalling in the development of axon, dendrites and synapses. *Open Biology* **8**:180116. doi:10.1098/rsob.180116

Hebb DO. 1949. The organization of behavior; a neuropsychological theory., The organization of behavior; a neuropsychological theory. Oxford, England: Wiley.

Hendi A, Mizumoto K. 2018. GFPnovo2 , a brighter GFP variant for in vivo labeling in C . elegans. *microPublication Biology*.

Herman MA, Vassilieva LL, Horvitz HR, Shaw JE, Herman RK. 1995. The C. elegans gene lin-44, which controls the polarity of certain asymmetric cell divisions, encodes a Wnt protein and acts cell nonautonomously. *Cell* **83**:101–110. doi:10.1016/0092-8674(95)90238-4

Hernandez F, Lucas JJ, Avila J. 2012. GSK3 and tau: Two convergence points in Alzheimer's disease. *Advances in Alzheimer's Disease* **3**:141–144. doi:10.3233/978-1-61499-154-0-141

Herr P, Basler K. 2012. Porcupine-mediated lipidation is required for Wnt recognition by Wls. *Developmental Biology* **361**:392–402. doi:10.1016/j.ydbio.2011.11.003

Hilliard MA, Bargmann CI. 2006. Wnt signals and Frizzled activity orient anterior-posterior axon outgrowth in C. elegans. *Developmental Cell* **10**:379–390. doi:10.1016/j.devcel.2006.01.013

Inaki M, Yoshikawa S, Thomas JB, Aburatani H, Nose A. 2007. Wnt4 Is a Local Repulsive Cue that Determines Synaptic Target Specificity. *Current Biology* **17**:1574–1579. doi:10.1016/j.cub.2007.08.013

Inestrosa NC, Montecinos-Oliva C, Fuenzalida M. 2012. Wnt signaling: Role in Alzheimer disease and schizophrenia. *Journal of Neuroimmune Pharmacology* **7**:788–807. doi:10.1007/s11481-012-9417-5

Innocenti GM, Ansermet F, Parnas J. 2003. Schizophrenia, neurodevelopment and corpus callosum. *Molecular Psychiatry* **8**:261–274. doi:10.1038/sj.mp.4001205

Jackson BM, Eisenmann DM. 2012. β-catenin-dependent wnt signaling in C. elegans: Teaching an old dog a new trick. *Cold Spring Harbor Perspectives in Biology* **4**:a007948. doi:10.1101/cshperspect.a007948

Jiang LI, Sternberg PW. 1998. Interactions of EGF, Wnt and HOM-C genes specify the P12 neuroectoblast fate in C. elegans. *Development (Cambridge, England)* **125**:2337–2347.

Kage E, Hayashi Y, Takeuchi H, Hirotsu T, Kunitomo H, Inoue T, Arai H, Iino Y, Kubo T. 2005. MBR-1, a novel helix-turn-helix transcription factor, is required for pruning excessive neurites in Caenorhabditis elegans. *Current Biology* **15**:1554–1559. doi:10.1016/j.cub.2005.07.057

Kanamori T, Kanai MI, Dairyo Y, Yasunaga K -i., Morikawa RK, Emoto K. 2013. Compartmentalized Calcium Transients Trigger Dendrite Pruning in Drosophila Sensory Neurons. *Science* **340**:1475–1478. doi:10.1126/science.1234879

Kantor DB, Kolodkin AL. 2003. Curbing the excesses of youth: Molecular insights into axonal pruning. *Neuron* **38**:849–852. doi:10.1016/S0896-6273(03)00364-7

Katanaev VL, Ponzielli R, Sémériva M, Tomlinson A. 2005. Trimeric G protein-dependent frizzled signaling in Drosophila. *Cell* **120**:111–122. doi:10.1016/j.cell.2004.11.014

Katsu T, Ujike H, Nakano T, Tanaka Y, Nomura A, Nakata K, Takaki M, Sakai A, Uchida N, Imamura T, Kuroda S. 2003. The human frizzled-3 (FZD3) gene on chromosome 8p21, a receptor gene for Wnt ligands, is associated with the susceptibility to schizophrenia. *Neuroscience Letters* **353**:53–56. doi:10.1016/j.neulet.2003.09.017

Kerr KS, Fuentes-Medel Y, Brewer C, Barria R, Ashley J, Abruzzi KC, Sheehan A, Tasdemir-Yilmaz OE, Freeman MR, Budnik V. 2014. Glial wingless/wnt regulates glutamate receptor clustering and synaptic physiology at the Drosophila neuromuscular junction. *Journal of Neuroscience* **34**:2910–2920. doi:10.1523/JNEUROSCI.3714-13.2014

Kikuchi A, Yamamoto H, Sato A, Matsumoto S. 2011. New Insights into the Mechanism of Wnt Signaling Pathway ActivationInternational Review of Cell and Molecular Biology. Elsevier Inc. pp. 21–71. doi:10.1016/B978-0-12-386035-4.00002-1

Kirszenblat L, Pattabiraman D, Hilliard MA. 2011. LIN-44/Wnt Directs Dendrite Outgrowth through LIN-17/Frizzled in C. elegans Neurons. *PLoS Biology* **9**:e1001157. doi:10.1371/journal.pbio.1001157

Klassen MP, Shen K. 2007. Wnt Signaling Positions Neuromuscular Connectivity by Inhibiting Synapse Formation in C. elegans. *Cell* **130**:704–716. doi:10.1016/j.cell.2007.06.046

Kohn AD, Moon RT. 2005. Wnt and calcium signaling: β-Catenin-independent pathways. *Cell Calcium* **38**:439–446. doi:10.1016/j.ceca.2005.06.022

Kuo CT, Jan LY, Jan YN. 2005. Dendrite-specific remodeling of Drosophila sensory neurons requires matrix metalloproteases, ubiquitin-proteasome, and ecdysone signaling. *Proceedings of the National Academy of Sciences* **102**:15230–15235. doi:10.1073/pnas.0507393102

Lee H, Jan LY, Jan Y. 2009. P60-Like 1 Regulate Dendrite Pruning of Sensory Neuron During Metamorphosis. *Apoptosis* **1**:1–6.

Lee T, Lee A, Luo L. 1999. Development of the Drosophila mushroom bodies: sequential generation of three distinct types of neurons from a neuroblast. *Development (Cambridge, England)* **126**:4065–76.

Lee T, Marticke S, Sung C, Robinow S, Luo L. 2000. Cell-autonomous requirement of the USP/EcR-B ecdysone receptor for mushroom body neuronal remodeling in Drosophila. *Neuron* **28**:807–818. doi:10.1016/S0896-6273(00)00155-0

Levy-Strumpf N, Culotti JG. 2014. Netrins and Wnts Function Redundantly to Regulate Antero-Posterior and Dorso-Ventral Guidance in C. elegans. *PLoS Genetics* **10**. doi:10.1371/journal.pgen.1004381

Low LK, Liu X-B, Faulkner RL, Coble J, Cheng H-J. 2008. Plexin signaling selectively regulates the stereotyped pruning of corticospinal axons from visual cortex. *Proceedings of the National Academy of Sciences* **105**:8136–8141. doi:10.1073/pnas.0803849105

Luo L, O'Leary DDM. 2005. AXON RETRACTION AND DEGENERATION IN DEVELOPMENT AND DISEASE. *Annual Review of Neuroscience* **28**:127–156. doi:10.1146/annurev.neuro.28.061604.135632

Lyuksyutova AI, Lu CC, Milanesio N, King LA, Guo N, Wang Y, Nathans J, Tessier-Lavigne M, Zou Y. 2003. Anterior-Posterior Guidance of Commissural Axons by Wnt-Frizzled Signaling. *Science* **302**:1984–1988. doi:10.1126/science.1089610

Maes T, Barceló A, Buesa C. 2002. Neuron Navigator: A Human Gene Family with Homology to unc-53, a Cell Guidance Gene from Caenorhabditis elegans. *Genomics* **80**:21–30. doi:10.1006/geno.2002.6799

Maguschak KA, Ressler KJ. 2011. Wnt Signaling in Amygdala-Dependent Learning and Memory. *Journal of Neuroscience* **31**:13057–13067. doi:10.1523/jneurosci.3248-11.2011

Maro GS, Klassen MP, Shen K. 2009. A β-Catenin-Dependent Wnt Pathway Mediates Anteroposterior Axon Guidance in C. elegans Motor Neurons. *PLoS ONE* **4**:e4690. doi:10.1371/journal.pone.0004690

Mataix-Cols D, Cardoner N, Via E, Happé F, Radua J. 2011. Meta-analysis of Gray Matter Abnormalities in Autism Spectrum Disorder. *Archives of General Psychiatry* **68**:409. doi:10.1001/archgenpsychiatry.2011.27

McCaffery P, Deutsch CK. 2005. Macrocephaly and the control of brain growth in autistic disorders. *Progress in Neurobiology* **77**:38–56. doi:10.1016/j.pneurobio.2005.10.005

Mello CC, Kramer JM, Stinchcomb D, Ambros V. 1991. Efficient gene transfer in C.elegans: extrachromosomal maintenance and integration of transforming sequences. *The EMBO journal* **10**:3959–70.

Meyer RL. 1998. Roger Sperry and his chemoaffinity hypothesis. *Neuropsychologia* **36**:957–980. doi:10.1016/S0028-3932(98)00052-9

Miller JR. 2002. The Wnts. *Genome biology* **3**:REVIEWS3001. doi:10.1186/gb-2001-3-1-reviews3001

Miller KD, Abbott LF, Song S. 2000. Competitive Hebbian learning through spike-timing-dependent synaptic plasticity. *Nature Neuroscience* **3**:919–926.

Mizumoto K, Sawa H. 2007. Cortical β-Catenin and APC Regulate Asymmetric Nuclear β-Catenin Localization during Asymmetric Cell Division in C. elegans. *Developmental Cell* **12**:287–299. doi:10.1016/j.devcel.2007.01.004

Mizumoto K, Shen K. 2013. Two Wnts Instruct Topographic Synaptic Innervation in C. elegans. *Cell Reports* **5**:389–396. doi:10.1016/j.celrep.2013.09.011

Moti N, Yu J, Boncompain G, Perez F, Virshup DM. 2019. Wnt traffic from endoplasmic reticulum to filopodia. *PLOS ONE* **14**:e0212711. doi:10.1371/journal.pone.0212711

Niell CM, Meyer MP, Smith SJ. 2004. In vivo imaging of synapse formation on a growing dendritic arbor. *Nature Neuroscience* **7**:254–260. doi:10.1038/nn1191

Norris AD, Lundquist EA. 2011. UNC-6/netrin and its receptors UNC-5 and UNC-40/DCC modulate growth cone protrusion in vivo in C. elegans. *Development* **138**:4433–4442. doi:10.1242/dev.068841

Nusse R, Varmus HE. 1992. Wnt genes. *Cell* **69**:1073–1087. doi:10.1016/0092-8674(92)90630-U

Nusse R, Varmus HE. 1982. Many tumors induced by the mouse mammary tumor virus contain a provirus integrated in the same region of the host genome. *Cell* **31**:99–109. doi:10.1016/0092-8674(82)90409-3

Obinata H, Sugimoto A, Niwa S. 2018. Streptothricin acetyl transferase 2 (Sat2): A dominant selection marker for Caenorhabditis elegans genome editing. *PLOS ONE* **13**:e0197128. doi:10.1371/journal.pone.0197128

Packard M, Koo ES, Gorczyca M, Sharpe J, Cumberledge S, Budnik V. 2002. The Drosophila Wnt, Wingless, Provides an Essential Signal for Pre- and Postsynaptic Differentiation. *Cell* **111**:319–330. doi:10.1016/S0092-8674(02)01047-4

Pan C, Howell JE, Clark SG, Hilliard M, Cordes S, Bargmann CI, Garriga G. 2006. Multiple Wnts and Frizzled Receptors Regulate Anteriorly Directed Cell and Growth Cone Migrations in Caenorhabditis elegans. *Developmental Cell* **10**:367–377. doi:10.1016/j.devcel.2006.02.010

Pani AM, Goldstein B. 2018. Direct visualization of a native Wnt in vivo reveals that a long-range Wnt gradient forms by extracellular dispersal. *eLife* **7**:1–22. doi:10.7554/elife.38325

Pfeiffenberger C, Yamada J, Feldheim DA. 2006. Ephrin-As and Patterned Retinal Activity Act Together in the Development of Topographic Maps in the Primary Visual System. *Journal of Neuroscience* **26**:12873–12884. doi:10.1523/JNEUROSCI.3595-06.2006

Richmond JE, Davis WS, Jorgensen EM. 1999. UNC-13 is required for synaptic vesicle fusion in C. elegans. *Nature Neuroscience* **2**:959–964. doi:10.1038/14755

Routledge D, Scholpp S. 2019. Mechanisms of intercellular Wnt transport. *Development* **146**:dev176073. doi:10.1242/dev.176073

Saha S, Aranda E, Hayakawa Y, Bhanja P, Atay S, Brodin NP, Li J, Asfaha S, Liu L, Tailor Y, Zhang J, Godwin AK, Tome WA, Wang TC, Guha C, Pollard JW. 2016. Macrophage-derived extracellular vesicle-packaged WNTs rescue intestinal stem cells and enhance survival after radiation injury. *Nature Communications* **7**:13096. doi:10.1038/ncomms13096

Sahores M, Gibb A, Salinas PC. 2010. Frizzled-5, a receptor for the synaptic organizer Wnt7a, regulates activity-mediated synaptogenesis. *Development* **137**:2215–2225. doi:10.1242/dev.046722

Saied-Santiago K, Townley RA, Attonito JD, da Cunha DS, Díaz-Balzac CA, Tecle E, Bülow HE. 2017. Coordination of Heparan Sulfate Proteoglycans with Wnt Signaling To Control Cellular Migrations and Positioning in Caenorhabditis elegans. *Genetics* **206**:1951–1967. doi:10.1534/genetics.116.198739

Schuldiner O, Yaron A. 2015. Mechanisms of developmental neurite pruning. *Cellular and Molecular Life Sciences* **72**:101–119. doi:10.1007/s00018-014-1729-6

Schumacher JA, Hsieh Y-W, Chen S, Pirri JK, Alkema MJ, Li W-H, Chang C, Chuang C-F. 2012. Intercellular calcium signaling in a gap junction-coupled cell network establishes asymmetric neuronal fates in C. elegans. *Development* **139**:4191–4201. doi:10.1242/dev.083428

Serralbo O, Marcelle C. 2014. Migrating cells mediate long-range WNT signaling. *Journal of Cell Science* **127**:e1.2-e1. doi:10.1242/jcs.155705

Shi Y, Li Q, Shao Z. 2018. Wnts Promote Synaptic Assembly Through T-Cell Specific Transcription Factors in Caenorhabditis elegans. *Frontiers in Molecular Neuroscience* **11**:1–14. doi:10.3389/fnmol.2018.00194

Singh AP, VijayRaghavan K, Rodrigues V. 2010. Dendritic refinement of an identified neuron in the Drosophila CNS is regulated by neuronal activity and Wnt signaling. *Development* **137**:1351–1360. doi:10.1242/dev.044131

Singh KK, Ge X, Mao Y, Drane L, Meletis K, Samuels BA, Tsai LH. 2010. Dixdc1 is a critical regulator of disc1 and embryonic cortical development. *Neuron* **67**:33–48. doi:10.1016/j.neuron.2010.06.002

Slusarski D. C., Corces VG, Moon RT. 1997. Interaction of Wnt and a Frizzled homologue triggers G-protein-linked phosphatidylinositol signalling. *Nature* **390**:410–413. doi:10.1038/37138

Slusarski Diane C., Yang-Snyder J, Busa WB, Moon RT. 1997. Modulation of embryonic intracellular Ca2+ signaling by Wnt-5A. *Developmental Biology* **182**:114–120. doi:10.1006/dbio.1996.8463

Smith CJ, Watson JD, Spencer WC, O'Brien T, Cha B, Albeg A, Treinin M, Miller DM. 2010. Time-lapse imaging and cell-specific expression profiling reveal dynamic branching and molecular determinants of a multi-dendritic nociceptor in C. elegans. *Developmental Biology* **345**:18–33. doi:10.1016/j.ydbio.2010.05.502

Stanganello E, Hagemann AIH, Mattes B, Sinner C, Meyen D, Weber S, Schug A, Raz E, Scholpp S. 2015. Filopodia-based Wnt transport during vertebrate tissue patterning. *Nature Communications* **6**:1–14. doi:10.1038/ncomms6846

Strigini M, Cohen SM. 2000. Wingless gradient formation in the Drosophila wing. *Current Biology* **10**:293–300. doi:10.1016/S0960-9822(00)00378-X

Struhl G, Casal J, Lawrence PA. 2012. Dissecting the molecular bridges that mediate the function of Frizzled in planar cell polarity. *Development (Cambridge, England)* **139**:3665–3674. doi:10.1242/dev.083550

Sulston JE, Horvitz HR. 1977. Post-embryonic cell lineages of the nematode, Caenorhabditis elegans. *Developmental Biology* **56**:110–156. doi:10.1016/0012-1606(77)90158-0

Sulston JE, Schierenberg E, White JG, Thomson JN. 1983. The embryonic cell lineage of the nematode Caenorhabditis elegans. *Developmental Biology* **100**:64–119. doi:10.1016/0012-1606(83)90201-4

Supekar K, Uddin LQ, Khouzam A, Phillips J, Gaillard WD, Kenworthy LE, Yerys BE, Vaidya CJ, Menon V. 2013. Brain Hyperconnectivity in Children with Autism and its Links to Social Deficits. *Cell Reports* **5**:738–747. doi:10.1016/j.celrep.2013.10.001

Tamai K, Semenov M, Kato Y, Spokony R, Liu C, Katsuyama Y, Hess F, Saint-Jeannet J-P, He X. 2000. LDL-receptor-related proteins in Wnt signal transduction. *Nature* **407**:530–535. doi:10.1038/35035117

Thomas-Virnig CL, Sims PA, Simske JS, Hardin J. 2004. The Inositol 1,4,5-Trisphosphate Receptor Regulates Epidermal Cell Migration in Caenorhabditis elegans. *Current Biology* **14**:1882–1887. doi:10.1016/j.cub.2004.10.001

Tian A, Duwadi D, Benchabane H, Ahmed Y. 2019. Essential long-range action of Wingless/Wnt in adult intestinal compartmentalization. *PLOS Genetics* **15**:e1008111. doi:10.1371/journal.pgen.1008111

Tree DRP, Shulman JM, Scott MP, Gubb D, Axelrod JD. 2002. to Generate Asymmetric Planar Cell Polarity Signaling. *Cell* **109**:371–381. doi:http://dx.doi.org/10.1016/S0092-8674(02)00715-8

Usui T, Shima Y, Shimada Y, Hirano S, Burgess RW, Schwarz TL, Takeichi M, Uemura T. 1999. Flamingo, a seven-pass transmembrane cadherin, regulates planar cell polarity under the control of Frizzled. *Cell* **98**:585–595. doi:10.1016/S0092-8674(00)80046-X

Vázquez-Manrique RP, Nagy AI, Legg JC, Bales OAM, Ly S, Baylis HA. 2008. Phospholipase C-ε Regulates Epidermal Morphogenesis in Caenorhabditis elegans. *PLoS Genetics* **4**:e1000043. doi:10.1371/journal.pgen.1000043

Walker DS, Vázquez-Manrique RP, Gower NJD, Gregory E, Schafer WR, Baylis HA. 2009. Inositol 1,4,5-trisphosphate signalling regulates the avoidance response to nose touch in Caenorhabditis elegans. *PLoS Genetics* **5**:1–10. doi:10.1371/journal.pgen.1000636

Walker DS, Yan G, Towlson EK, Schafer WR, Barabási A-L, Chew YL, Vértes PE. 2017. Network control principles predict neuron function in the Caenorhabditis elegans connectome. *Nature* **550**:519–523. doi:10.1038/nature24056

Watts RJ, Hoopfer ED, Luo L. 2003. Axon Pruning during Drosophila Metamorphosis. *Neuron* **38**:871–885. doi:10.1016/S0896-6273(03)00295-2

Wenick AS, Hobert O. 2004. Genomic cis-regulatory architecture and trans-acting regulators of a single interneuron-specific gene battery in C. elegans. *Developmental Cell* **6**:757–770. doi:10.1016/j.devcel.2004.05.004

Whangbo J, Kenyon C. 1999. A Wnt Signaling System that Specifies Two Patterns of Cell Migration in C. elegans. *Molecular Cell* **4**:851–858. doi:10.1016/S1097-2765(00)80394-9

White JG, Southgate E, Thomson JN, Brenner S. 1986. The Structure of the Nervous System of the Nematode Caenorhabditis elegans. *Philosophical Transactions of the Royal Society B: Biological Sciences* **314**:1–340. doi:10.1098/rstb.1986.0056

Willert K, Brown JD, Danenberg E, Duncan AW, Weissman IL, Reya T, Yates JR, Nusse R. 2003. Wnt proteins are lipid-modified and can act as stem cell growth factors. *Nature* **423**:448–452. doi:10.1038/nature01611

Williams DW, Truman JW. 2005. Cellular mechanisms of dendrite pruning in Drosophila: insights from in vivo time-lapse of remodeling dendritic arborizing sensory neurons. *Development (Cambridge, England)* **132**:3631–42. doi:10.1242/dev.01928

Wolff T, Rubin GM. 1998. Strabismus, a novel gene that regulates tissue polarity and cell fate decisions in Drosophila. *Development (Cambridge, England)* **125**:1149–59.

Wong H-C, Bourdelas A, Krauss A, Lee H-J, Shao Y, Wu D, Mlodzik M, Shi D-L, Zheng J. 2003. Direct Binding of the PDZ Domain of Dishevelled to a Conserved Internal Sequence in the C-Terminal Region of Frizzled activity and stabilization of -catenin in the cytoplasm, is essential for the specification of cell fate in Drosophila and Xenopus. The . *Molecular Cell* **12**:1251–1260.

Wu GY, Zou DJ, Rajan I, Cline H. 1999. Dendritic Dynamics In Vivo Change during Neuronal Maturation . *The Journal of Neuroscience* **19**:4472–4483. doi:10.1523/jneurosci.19-11-04472.1999

Wu M, Herman MA. 2007. Asymmetric localizations of LIN-17/Fz and MIG-5/Dsh are involved in the asymmetric B cell division in C. elegans. *Developmental Biology* **303**:650–662. doi:10.1016/j.ydbio.2006.12.002

Xu NJ, Henkemeyer M. 2009. Ephrin-B3 reverse signaling through Grb4 and cytoskeletal regulators mediates axon pruning. *Nature Neuroscience* **12**:268–276. doi:10.1038/nn.2254

Yamamoto Y, Takeshita H, Sawa H. 2011. Multiple Wnts Redundantly Control Polarity Orientation in Caenorhabditis elegans Epithelial Stem Cells. *PLoS Genetics* **7**:e1002308. doi:10.1371/journal.pgen.1002308

Yang Y, Mlodzik M, Biology R. 2016. HHS Public Access. *Annu Rev Cell Dev Biol* **116**:623–646. doi:10.1146/annurev-cellbio-100814-125315.Wnt-Frizzled/Planar

Yoshikawa S, McKinnon RD, Kokel M, Thomas JB. 2003. Wnt-mediated axon guidance via the Drosophila derailed receptor. *Nature* **422**:583–588. doi:10.1038/nature01522

Yu J, Chia J, Canning CA, Jones CM, Bard FA, Virshup DM. 2014. WLS Retrograde transport to the endoplasmic reticulum during Wnt secretion. *Developmental Cell* **29**:277–291. doi:10.1016/j.devcel.2014.03.016

Yu XM, Gutman I, Mosca TJ, Iram T, Özkan E, Garcia KC, Luo L, Schuldiner O. 2013. Plum, an immunoglobulin superfamily protein, regulates axon pruning by facilitating TGF-β signaling. *Neuron* **78**:456–468. doi:10.1016/j.neuron.2013.03.004

Zanardelli S, Christodoulou N, Skourides PA. 2013. Calpain2 protease: A new member of the Wnt/Ca2+pathway modulating convergent extension movements in Xenopus. *Developmental Biology* **384**:83–100. doi:10.1016/j.ydbio.2013.09.017

Zecca M, Basler K, Struhl G. 1996. Direct and Long-Range Action of a Wingless Morphogen Gradient. *Cell* **87**:833–844. doi:10.1016/S0092-8674(00)81991-1

Zheng X, Wang J, Haerry TE, Y-H Wu A, Martin J, O MB, Lee C-HJ, Lee T, Wu AY, Martin J, Connor MBO, Lee C-HJ, Lee T. 2003. TGF-Signaling Activates Steroid Hormone Receptor Expression during Neuronal Remodeling in the Drosophila Brain (Iyengar and Bottjer,

2002). Understanding the genetic programs that control neuronal plasticity may help develop strategies for manipulating n, Cell.